# Regulation and Endogenous Activators of the Cell-Intrinsic Antiviral Response

Sterling Clay Eckard

A dissertation
submitted in partial fulfillment of the
requirements for the degree of

Doctor of Philosophy

University of Washington

2014

Reading Committee:
Daniel B. Stetson, Chair
Keith B. Elkon
Ram Savan

Program Authorized to Offer Degree:
Department of Immunology

University of Washington

## Abstract

Regulation and Endogenous Activators of the Cell-Intrinsic Antiviral Response

Sterling Clay Eckard

Chair of Supervisory Committee:
Associate Professor Daniel B. Stetson
Department of Immunology

The primary objective of immune sensors is to differentiate self from non-self. Detection of viral genomes leads to activation of the antiviral response, accompanied by the production of type I interferons. However, these viral nucleic acids are very similar to host produced RNA and DNA. We investigate how human variants in SKIV2L, an RNA metabolism enzyme, can lead to erroneous interferon production by allowing an accumulation of self-RNA. While studying sources of the endogenous ligands that can accumulate, we considered the role of RNase L in the antiviral response. While the OAS/2-5A system and RNase L have been studied for many years, our findings suggest a new model for their function. We reveal that RNase L acts as a negative regulator of the antiviral response by eliciting global translational inhibition through cleavage of ribosomal RNA. We go on to show that the different 2-5A species synthesized by OAS proteins are endogenous immunostimulatory ligands, and that the OAS/2-5A system generates ligands for crosstalk between the RNA and DNA sensing and signaling networks within every cell. These studies have far-reaching implications for the detection of endogenous RNA ligands, their metabolism, and their association with autoimmune disorders. Furthermore, the reappraisal of RNase L and the new role for 2-5A species as endogenous activators of the antiviral response come with their own clinical implications, and allow for a more complete understanding of the early cellular response to viral pathogens.

# Table of Contents

## Acknowledgements

The author would like to express his sincere gratitude for everyone's support throughout graduate school. In particular, I would like to thank Dan Stetson for his excellent mentorship and subsequent friendship throughout my graduate career. Thanks also go to Steve Ziegler for 'finding me on his doorstep' and giving me a chance. The entire Stetson lab, past and present, has been a fantastic and inspiring group to work with – so thank you all. My classmates made the whole process humbling and exciting, and we've become a science family along the way. I appreciate the support of my committee members: Keith Elkon, Michael Gale, Jr., Andrew Oberst, Ram Savan, and Jason Smith. Acknowledgement goes to Jon Clingan for assisting with the RNase L project and performing the polysome analysis. Additional collaborators are David Barton and Daphne cooper, who performed RNA sequencing experiments on RNase L samples. Finally, my family and my friends… you're the best.

## Dedication

A mother, a father, and a boy make three.

## Glossary

2-5A: 2’-5’-linked oligoadenylate

AGS: Aicardi-Goutières Syndrome

BMDM: Bone marrow-derived macrophage

CARD: Caspase recruitment domains

CDN: Cyclic dinucleotides

cGAMP: Cyclic GMP-AMP

cGAS: Cyclic GMP-AMP synthetase

DMXAA: 5,6-dimethylxanothenone-4-acetic acid

dsRNA: Double stranded RNA

ER: Endoplasmic reticulum

HPC1: Hereditary prostate cancer locus 1

IFN: Interferon

IFNαR: Interferon-alpha receptor

IRE1: Inositol-requiring protein 1

ISD: Interferon-stimulatory DNA

ISG: Interferon-stimulated gene

LPS: Lipopolysaccharide

MAVS: Mitochondrial antiviral signaling

MDA5: Melanoma differentiation-associated protein 5

MEF: Murine embryonic fibroblast

OAS: Oligoadenylate synthetase

PAMP: Pattern associated molecular pattern

PKR: Protein kinase R

PRR: Pattern recognition receptor

RNase L: Ribonuclease L

RIDD: Regulated IRE-1 dependent RNA decay

RIG-I: Retinoic acid-inducible gene I

RLR: RIG-I-like receptor

RQ: Relative quantification

rRNA: Ribosomal RNA

SERCA: Sarco/endoplasmic reticulum calcium ATPase

SKIV2L: Superkiller viralicidic activity 2-like

SLE: Systemic lupus erythematosus

ssRNA: Single stranded RNA

STING: Stimulator of interferon genes

THES: Trichohepatoenteric syndrome

TLR: Toll-like receptor

TNF: Tumor necrosis factor

Trex1: 3’ repair exonuclease 1

TTC37: Tetratricopeptide repeat protein 37

UMI: Unique molecular identifier

UPR: Unfolded protein response

VSV: Vesicular stomatitis virus

WT: Wild-type

XBP1: X-box-binding protein 1

XRN1: 5’-3’ exoribonuclease 1

# Chapter 1: Introduction

## Defining Crosstalk Between Stress Responses and Innate Immunity

Every day, viruses in our environment try to infect the cells in our body and replicate. Our cells have defensive machinery designed to detect and stop viral infections, generating inflammation that alerts neighboring cells. The vertebrate immune system must also handle the burden of multicellularity, which requires the compartmentalization of cellular patrols and inflammatory responses to pathogen insults. This system must be carefully balanced, or the system, which has evolved to protect us, can cause great harm to our own tissues. All cells have sensors that detect foreign nucleic acids and trigger a cell-intrinsic antiviral response through the production of type I interferons[1,2]. The RNA helicases RIG-I and MDA5 detect viral RNA in a sequence non-specific manner based on structural motifs, while the sensors for DNA viruses are still being fully explored[3,4]. These sensors require careful regulation because they must be sensitive to small amounts of viral nucleic acid while not reacting to the abundance of self-RNA and DNA within all cells. In addition to viral ligands, these sensors can also potentially react to endogenous nucleic acids and elicit an antiviral response[5]. Chronic activation of the cell-intrinsic antiviral response by these endogenous ligands causes fatal autoimmune disease, underscoring the importance of this careful regulation[6].

## The Innate Immune System

The innate immune system is the body's first response against pathogen invasion. In the first minutes or hours after infection, innate sensors and cells mount a potent response that has profound influence over the downstream programing of the adaptive immune response. The innate immune system includes a variety of hematopoietic cells, all of which have specialized systems of recognition and response. Cell types include macrophages, dendritic cells, neutrophils, eosinophils, basophils, mast cells, and natural killer cells. These cells specialize in recognizing unique surface or nucleic acid motifs known as pathogen associated molecular patterns (PAMPs) using pattern recognition receptors (PRRs). These PRRs include toll-like receptors (TLRs), which can recognize viral DNA or RNA within a cell's endosomal compartments. Other classes of receptors include the RIG-I-like receptors (RLRs) and DNA

sensors, which, respectively, detect RNA and DNA in the cytoplasm[7]. Recognition of PAMPs leads to production of inflammatory cytokines and chemokines, phagocytosis, or killing. Cytokines and chemokines include tumor necrosis factor (TNF), interleukin 1ß (IL-1ß), and type I interferons such is interferons α and ß (IFNα, IFNß) among others. The type of pathogen recognized, and the cytokine profile mounted by these innate cells, will then define the adaptive immune response[8].

Of particular importance to the work presented here are the intracellular PRRs for viral RNA. These are RIG-I and MDA5, and, when activated by bound ligand, trigger downstream antiviral responses through the generation of type I interferons (**Fig. 1.1**; [9,10]). These receptors each contain C-terminal DExD/H box-containing RNA helicase domains that are responsible for binding RNA. Once RNA is bound, signaling is achieved through protein-protein interactions with mitochondrial antiviral signaling (MAVS), moderated by the N-terminal caspase recruitment domains (CARDs)[11-13]. These receptors are not restricted to innate immune cells, but instead are present in almost every cell type in our bodies. This is paramount to generating a strong and swift response to a viral infection, but it also means that such a response must be very carefully regulated. Any erroneous activation would spell trouble for the host organism. There are several examples of autoimmune disease pathology dependent on increased type I interferon levels, including systemic lupus erythematosus (SLE), and Sjögren's syndrome[14-16].

The first cytokine produced upon viral detection, and the focus of much of the work presented here, is IFNß, and this cytokine can be produced by any cell in the body. IFNß production has rapid autocrine effects to make a cell less hospitable for viral replication, and it has quick paracrine effects on neighboring cells upon binding the interferon-alpha receptors 1 and 2 (IFNαR1, IFNαR2). A virus can infect any cell in the body, and so it is necessary that all cells are capable of mounting a response[17-19].

**Negative Regulation of Nucleic Acids**

Where do the endogenous nucleic acid ligands for intracellular antiviral sensors come from? In the case of the DNA-activated antiviral response called the interferon-stimulatory DNA (ISD) pathway, the Trex1 DNA exonuclease metabolizes the DNA ligands that trigger the ISD sensors. The primary source of these ISD ligands is reverse-transcribed DNA derived from endogenous retroelements, which

comprise half of the DNA content of the human genome, and can be activated by cellular stresses such as DNA damage. Trex1-deficient humans develop a severe lupus-related autoimmune disease called Aicardi-Goutieres Syndrome (AGS), demonstrating the importance of removing these ligands from within cells[5]. These findings establish two important concepts: endogenous nucleic acids can trigger autoimmune disease in the absence of infection, and specific enzymes exist to limit activation of the ISD pathway. What isn't established, however, is whether an analogous mechanism of intracellular RNA metabolism regulates the RIG-I-like receptors (RLRs) RIG-I and MDA5.

Outside of viral recognition and clearance, endogenous nucleic acids must be managed within the cell to avoid erroneous detection. The RNA exosome is responsible for metabolism of self nucleic acids, and does so by degrading RNA through a coordinated effort by a multiprotein complex[20-23]. Work is ongoing to understand the many roles of processing and surveillance in both nuclear and cytoplasmic compartments, but what is clear is that this concerted effort is essential to manage the accumulation of 'self' nucleic acids. The majority of studies on the RNA exosome have been performed in yeast due to the ease with which individual components can be deleted by genetic manipulation, so there are still many questions that remain regarding the mechanisms employed for localization and targeting in metazoans. The following work aims to elucidate the importance of specific enzymes and the role they play in keeping cellular RNAs from reaching a threshold that can activate the PRRs RIG-I and MDA5. Many technological challenges were overcome in the process of evaluating the impact of the RNA exosome on activation of the antiviral sensors, but much work remains to be done to address the new questions raised by these studies.

**Cell Stress**

We considered broadly the connections between cellular stress responses and innate immunity. Stress responses are defined as the detection of perturbations in homeostasis, including heat shock, hypoxia, DNA damage, and so on. Each stressor has specific sensors that activate a gene expression program to restore homeostasis, or, if the damage is too severe, commit to apoptosis[24]. Importantly, stress responses can be activated both by sterile insults and by infection, and in both cases the trigger is identical. One such example is the unfolded protein response (UPR), which is activated when

proteins accumulate in the endoplasmic reticulum (ER) in excess of ER protein folding capacity[25]. The UPR activates expression of genes that expand the size and chaperone content of the ER. This response has been extensively characterized in the context of sterile stress, for example during plasma B cell differentiation that converts an activated B cell into an antibody-secreting factory[26,27]. However, viral infections can also trigger the UPR through the unscheduled synthesis of envelope glycoproteins and capsid components. In this case, a "normal" UPR would actually favor viral production by expanding the ER. We hypothesize that, if they are not properly metabolized, specific RNA degradation products produced by the UPR can activate the RLRs. In the UPR, IRE1 is an ER-bound kinase/ribonuclease that is activated by protein accumulation, leading to oligomerization and trans-autophosphorylation that activates the endoribonuclease domain facing the cytosol. This leads to a unique cleavage of an intact intron in the Xbp1 mRNA[17]. The spliced form of Xbp1 is ligated by tRNA ligase, leading to the translation of a functional protein that acts as a transcription factor for downstream UPR events[28-30].

Studies have shown that the RNA endonuclease IRE1, a primary response element in the UPR, can generate 3'-cyclic phosphate RNA cleavage products which are believed to activate RIG-I[31-33]. We found that the 3'->5' RNA exosome, a heterotrimeric protein complex involved in RNA turnover, is a potent negative regulator of the RIG-I/MDA5 pathway. Knockdown of SKIV2L, an essential component of the RNA exosome and a recently described lupus susceptibility allele, resulted in massive enhancement of the antiviral response to RNA ligands[34,35].

**Human Variants of SKIV2L and Functional Consequences**

Recent studies have shown that rare human mutations in RNA exosome components cause a disease called Trichohepatoenteric Syndrome (THES)[36,37]. Patients were originally diagnosed with syndromic diarrhea and malnutrition, and we have found recent evidence that there may also be aberrant immune activation. The original THES patients were found to have mutations in TTC37, which is another component of the 3'->5' RNA exosome. The remaining patients with identical symptoms and no mutation in TTC37 were eventually shown to have full loss of function mutations in SKIV2L[38-40]. Pathology of the disease is thought to be primarily due to the generic defects of impaired RNA metabolism. Upon closer inspection, we were able to determine that there was also a considerable

increase in type I interferon scores in peripheral blood. This leads to interesting, unanswered, questions over the potentially differential roles of these different 3'->5' exosome components (**Fig. 1.2**). We believe that SKIV2L metabolizes endogenous RNA ligands of RIG-I/MDA5 to keep them below a threshold where they are able to activate viral RNA sensors. Polymorphisms in SKIV2L in people might generate chronic low-level inflammation that contributes to interferon-associated autoimmune disorders like lupus or type 1 diabetes.

**Different Sources of Endogenous Ligands**

RNase L is a well-characterized component of the antiviral response to RNA viruses[41,42]. RNase L is the product of an evolutionary duplication event, and the catalytic domains of both enzymes are very closely related[43]. RNAseL has also been associated with increased hereditary prostate cancer risk as a candidate for the HPC1 gene[44-46]. Once activated, RNase L dimerizes and becomes a functional endonuclease targeting single-stranded RNAs[47]. The current model of RNase L describes its indiscriminate cleavage of mRNA, tRNA, rRNA, and vRNA as being essential to its role as a positive regulator of RIG-I and the subsequent downstream type-I IFN response (**Fig. 1.3**). In the absence of RNase L, the IFN response is thought to be reduced, and these knockout mice have attenuated viral clearance[33,48]. A role for RNAseL in the innate antiviral response has not been characterized outside of its generation of RIG-I activating cleavage products.

Interestingly, the original observations made in 1974 surrounding the discovery of RNase L had a much different impression of the events that followed RNase L activation. Experiments showed that interferon treatment resulted in an inducible enzymatic activity that degraded RNA, presumably as a precautionary defense to viral infection[49,50]. It was hypothesized that infection and interferon production could bring about a general inhibition in protein translation. This was observed, showing that while cells might be more prone towards a death pathway, they produced little virus. We have since performed experiments supporting these original observations of RNase L function, and show convincingly that the true role of RNase L in the antiviral response is to localize to and specifically target ribosomal RNA for cleavage. This targeted cleavage has a global influence on protein translation to block viral replication, but also regulates the production of antiviral cytokines (**Fig. 1.4**).

**Other Sensors and Crosstalk Between the RNA and DNA Antiviral Pathways**

Other receptors important to the RNA and DNA antiviral response, respectively, are the oligoadenylate synthetase (OAS) proteins and cyclic GMP-AMP synthetase (cGAS). Current studies have highlighted the parallels in structure and function between these two template-independent nucleotidyltransferases, though their roles in the antiviral response are functionally distinct[51,52]. The OAS proteins (OAS1, OAS2, OAS3) are type I interferon-inducible, and catalytic activity is initiated upon binding double-stranded RNA. This activation is responsible for synthesizing 2'-5'-oligoadenylates (2-5A), and the only known biological function of 2-5A is to bind and activate RNase L[53].

cGAS is a recently identified detector of cytosolic DNA, and is an important piece of the puzzle in how the innate immune system is able to detect microbial pathogens. Upon binding with DNA, cGAS is activated and generates the unique second messenger molecule cyclic GMP-AMP (cGAMP) which directly binds to the endoplasmic reticulum adaptor protein, stimulator of IFN genes (STING)[54]. Activation of STING by cGAMP, or the bacterial cyclic dinucleotides (CDNs) cyclic-di-AMP (c-di-AMP) and cyclic-di-GMP (c-di-GMP), leads to the induction of IFNß[55]. This DNA sensing pathway acts in concert with the RNA sensing pathway in which MAVS is the signaling adaptor for RIG-I and MDA5. The functional similarities of cGAS and OAS become quite interesting, as both cGAS and the OAS proteins generate a 2'-5'-linked antiviral dinucleotide, and crosstalk between the two host second messenger pathways has not been previously considered (**Fig. 1.5**; [56]).

Our recent work considers the possibility that different OAS PRRs might have a more deliberate role in guiding the downstream immune response to RNA viruses by production of different species of 2-5A. It has been shown that OAS1 preferentially produces a 2-5A trimer, OAS2 a tetramer and pentamer, and OAS3 a dinucleotide, but the functional consequences of these different species has not been directly evaluated[57,58]. Our preliminary observations have revealed two novel actions of 2-5A: that it can act directly as an immunostimulatory molecule, and that there might be functional specialization of 2-5A molecules to activate both arms of the antiviral response via MAVS and STING. If true, this opens the door for exciting new work and potentially reconciles odd findings in the current literature. Viral antagonism of an antiviral pathway has been used as both a discovery tool and as confirmation of

the pathway itself. In spite of that, there are unresolved observations implying crosstalk between the MAVS and STING pathways to RNA and DNA viruses. STING knockout mice have been shown to have a reduced inflammatory response to certain RNA viruses[59]. If these viruses antagonize important components of the RNA detection pathway, a 2-5A dinucleotide produced upon detection of viral RNA to activate STING would represent a useful functional redundancy to ensure a rapid response. Additionally, it has been shown that Dengue virus encodes a protease that cleaves STING[60]. A virus would not waste evolutionary energy to antagonize a host-signaling pathway that is not important for detection of that virus.

**Clinical Implications and Future Directions**

Both SKIV2L and RNase L have known genetic human variants associated with disease. While their functions differ wildly, both of these genes operate as regulators of the cell-intrinsic antiviral response. Beyond better understanding the different signaling pathways, we feel that our studies have direct clinical implications. The requirement for SKIV2L to maintain homeostasis in the wake of UPR activation becomes most relevant in the context of highly-secretory cells, like ß-islet cells in type 1 diabetes, or tear and salivary glands in Sjögren's syndrome. A polymorphism that reduces SKIV2L function could lead to accumulation of endogenous nucleic acids, generating a chronic low-grade inflammation that might be responsible for the break in tolerance that leads to disease pathology. Similarly, our observations on the OAS/2-5A/RNase L system have relevance to its association with prostate cancer. If there is disruption of RNase L and its negative regulation of antiviral cytokines, this could allow erroneous inflammation and contribute to the transformation of host cells. Additionally, compromising the ability of RNase L to bind 2-5A might allow naturally produced 2-5A species to directly bind and activate both STING and MAVS, again leading to excess inflammation in affected regions. Understanding these pathways will allow us to better diagnose patients before full clinical onset, and pave the road to preventing the diseases entirely.

## Chapter 1 Figures

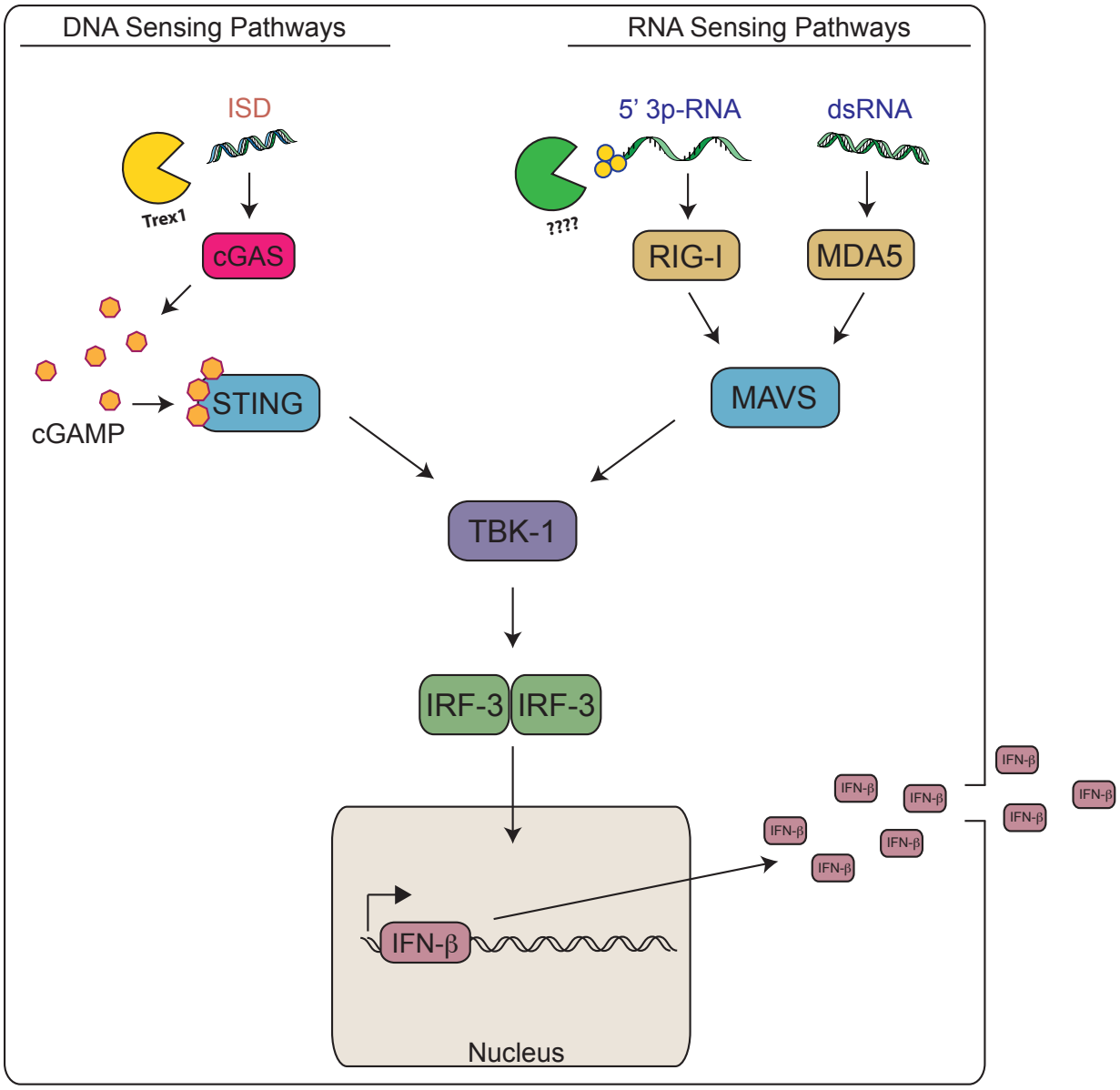


*Figure 1.1: Cell-intrinsic viral detection pathways*

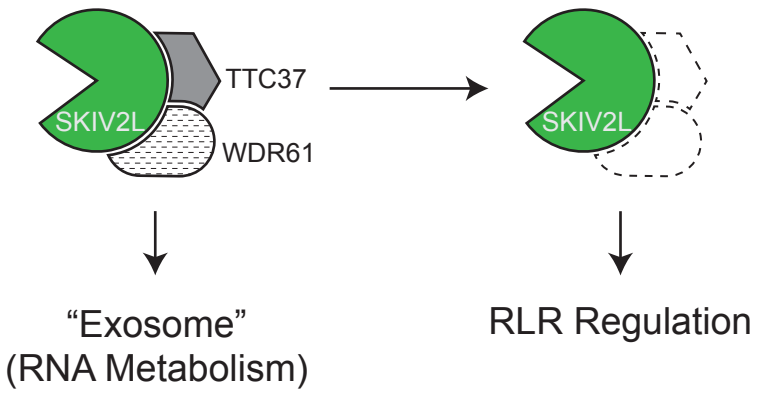


*Figure 1.2: Differential roles of SKIV2L in the RNA exosome*

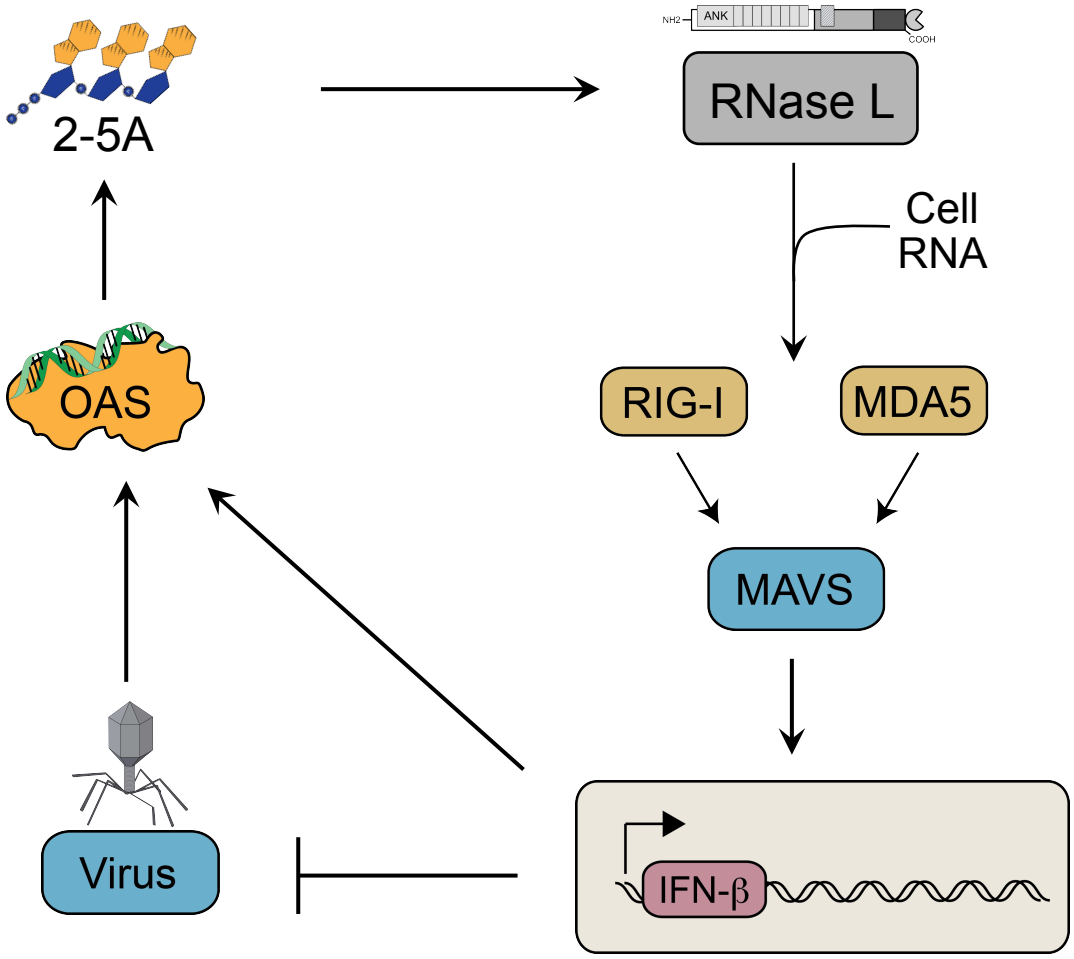


*Figure 1.3: Classical Model of RNase L Activation*

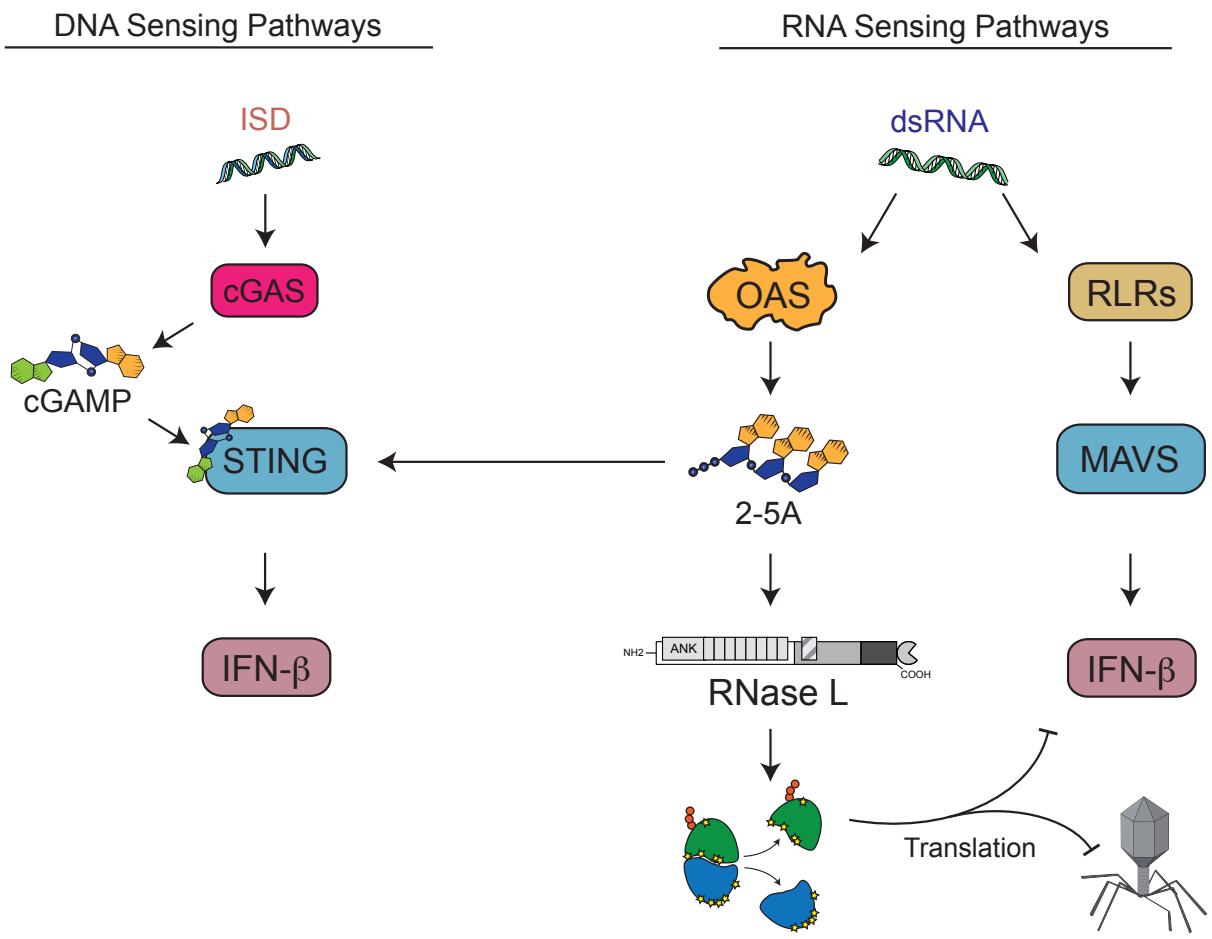


*Figure 1.4: Revised Model of RNase L Activation*

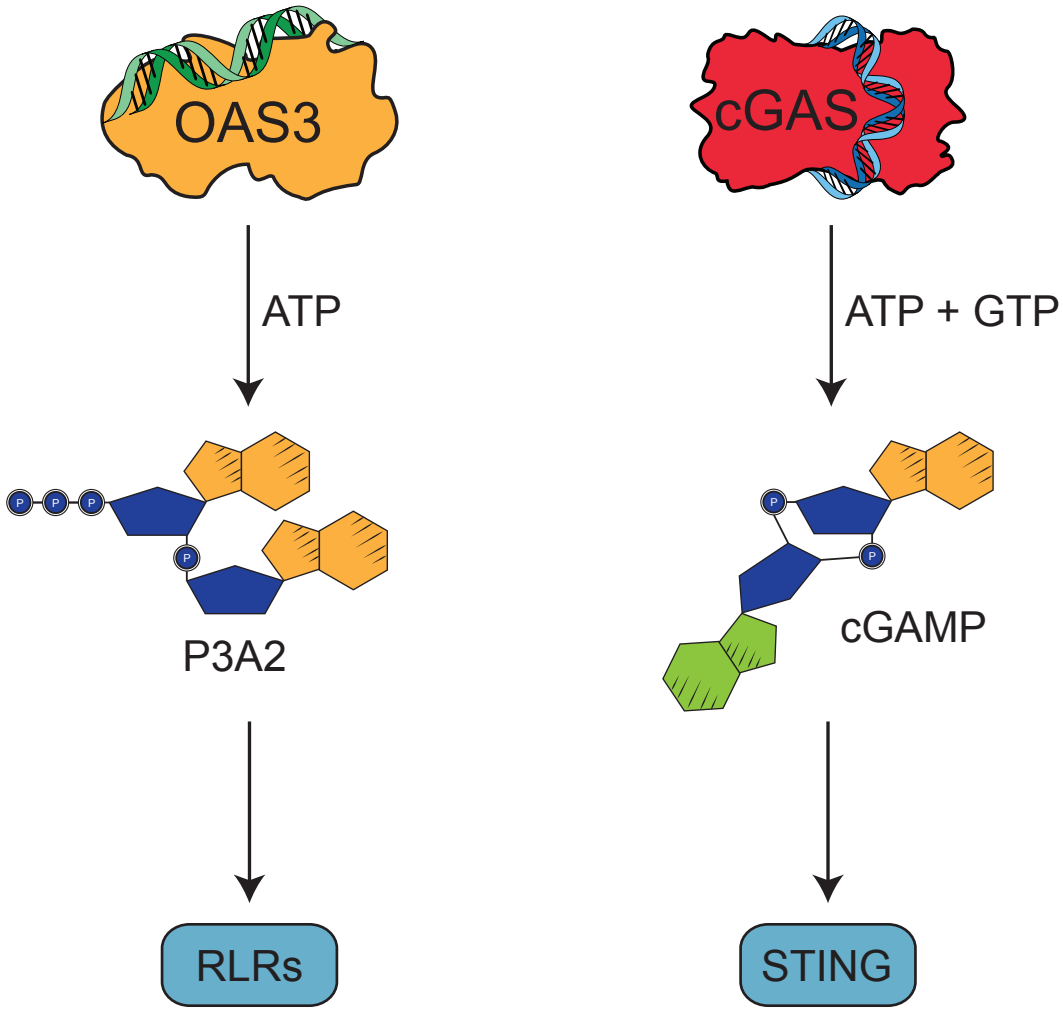


*Figure 1.5: Similarities of cGAS and OAS*

## Chapter 2: The SKIV2L RNA Exosome Limits Activation of the RIG-I-like Receptors

**Abstract**

Innate immune sensors of intracellular nucleic acids must be regulated to prevent inappropriate activation by endogenous DNA and RNA. The exonuclease Trex1 regulates the DNA sensing pathway by metabolizing potential DNA ligands that trigger it. However, an analogous mechanism for regulating the RIG-I-like receptors (RLRs) that detect RNA remains unknown. We show that the SKIV2L RNA exosome potently limits the activation of RLRs. We find that the unfolded protein response (UPR), which generates endogenous RLR ligands through IRE-1 endonuclease cleavage of cellular RNAs, triggers type I interferon (IFN) production in SKIV2L-depleted cells. Humans with SKIV2L deficiency have a type I IFN signature in their peripheral blood. Our findings reveal a mechanism for intracellular metabolism of immunostimulatory RNA, with implications for specific autoimmune disorders.

**Introduction**

Antiviral immunity is initiated within virus-infected cells by innate immune sensors of viral nucleic acids[4]. These sensors must detect viral RNA or DNA among a vast excess of cellular RNA and DNA, which presents a challenge of self/non-self discrimination and a risk of inappropriate immune responses to self nucleic acids. Specificity of these innate antiviral sensors is primarily accomplished by the detection of unique structural features that distinguish viral nucleic acids. For example, the RIG-I RNA helicase binds to 5′ triphosphate RNA that is present in the genomes of many classes of RNA viruses but scarce within host cells[61]. Similarly, the MDA5 RNA helicase is activated by long, double-stranded viral RNA that is not routinely formed in host cells[62]. For intracellular DNA sensing by the interferon stimulatory DNA (ISD) pathway, the mechanisms of self/non-self discrimination are less clear because the known DNA sensors are activated in a sequence-independent fashion by nearly any double-stranded DNA[54,63,64]. Indeed, recently published crystal structures of several important DNA receptors reveal that most molecular contacts with immunostimulatory DNA are made with the sugar-phosphate backbone and not the specific bases[65-67].

Recently, intracellular nucleic acid metabolism was identified as an essential mechanism for limiting the activation of the ISD pathway. We identified the 3′ repair exonuclease 1 (Trex1) in a biochemical screen for ISD-binding proteins[5]. Loss-of-function mutations in the human TREX1 gene cause Aicardi-Goutières syndrome (AGS), a severe type I interferon (IFN)-associated autoimmune disease[68]. Using Trex1-deficient mice as a model of AGS, we defined Trex1 as an essential negative regulator of the ISD pathway[5,69]. Moreover, we found that the reverse-transcribed cDNAs of endogenous retroelements accumulate within Trex1-deficient cells and that Trex1 is a potent anti-retroviral enzyme[5]. These studies provide a framework for understanding the pathogenic mechanisms of AGS and related diseases, and reveal an important source of endogenous intracellular nucleic acids that can trigger innate immune sensors of DNA if they fail to be properly metabolized.

Based on these findings, we wondered whether an analogous mechanism exists to metabolize intracellular RNA for regulation of the RIG-I-like receptors (RLRs), and whether there is a source of

relevant endogenous immunostimulatory RNAs that could trigger the RLRs upon their accumulation. We show here that the cytosolic 3′-to-5′ RNA exosome, defined by the SKIV2L RNA helicase, is an important negative regulator of the RLR-mediated antiviral response. We identify the RNA cleavage products of the inositol-requiring enzyme 1 (IRE-1) endonuclease as immunostimulatory RNAs that activate the RLR pathway in SKIV2L-depleted cells upon activation of the unfolded protein response (UPR). We show that SKIV2L-deficient humans have a type I IFN signature in their peripheral blood cells. These findings reveal a mechanism that may contribute to IFN-associated autoimmune diseases.

**Results**

*SKIV2L limits the RLR antiviral response*

We began our exploration of potential negative regulators of the RNA-activated antiviral response by considering the ubiquitous pathways for RNA degradation that mediate turnover of mRNAs and elimination of incompletely spliced RNA transcripts. These pathways are often initiated by endonucleolytic cleavage of the RNA, followed by degradation of the two resulting products by distinct enzyme complexes[70]. The XRN1 exonuclease metabolizes RNA in the 5′-to-3′ direction, and the RNA exosome degrades RNA in the 3′-to-5′ direction (**Fig. 2.1a**;[70]). The RNA exosome is a multi-protein complex composed of several core factors associated with key accessory proteins that determine its subcellular localization and RNA substrate specificity[22]. The RNA exosome responsible for RNA turnover in the cytoplasm of human cells is formed by the RNA helicase SKIV2L together with additional subunits that are well-characterized in yeast (SKI3, SKI8, ref. [71]) but remain poorly defined in humans. Intriguingly, a previous study identified *SKIV2L* as a potential susceptibility gene for the autoimmune disorder systemic lupus erythematosus (SLE) in humans[34]. We established stable, robust lentiviral knockdown of SKIV2L and XRN1 in primary mouse bone marrow-derived macrophages (BMDMs), confirming depletion of these proteins by western blot (**Fig. 2.1b**). We stimulated the knockdown cells by transfection of a pure triphosphate RNA ligand for RIG-I[72], and measured IFN-β mRNA transcription as the primary and most direct cytokine readout of RLR pathway activation. We found that SKIV2L-depleted cells exhibited a substantially enhanced IFN-β response to RIG-I ligands as compared to cells with scramble shRNA, and that XRN1 knockdown had no effect on IFN-β production (**Fig. 2.1c**). SKIV2L-depleted cells also had an enhanced IFN-β response to transfection of poly(I:C), which activates both RIG-I and MDA5 (**Fig. 2.1c**). The abundance of mRNAs encoding IFNα4, the inflammatory chemokine CXCL10 and interleukin 6 (IL-6), were similarly enhanced in SKIV2L-depleted cells but not XRN-1-depleted cells after RIG-I ligand stimulation (**Fig. 2.1d-f**), demonstrating broad enhancement of the RLR-activated antiviral response conferred by SKIV2L knockdown.

The enhancement of the antiviral response in SKIV2L-depleted cells could be a result of increased mRNA stability conferred by loss of a key participant in the regulation of mRNA turnover. To

control for the specificity of SKIV2L depletion, we stimulated cells with two non-nucleic acid ligands that each potently induce the type I IFN response. The chemotherapeutic agent 5,6-dimethylxanthenone-4-acetic acid (DMXAA) binds to and activates the STING adapter protein[73,74], and lipopolysaccharide (LPS) triggers IFN-β expression through the TLR4-Trif pathway[75]. We found that SKIV2L-depleted cells did not exhibit enhanced responses to these non-RNA ligands (**Fig. 2.1g,h**). These data suggest that SKIV2L is a specific negative regulator of the RNA-activated RLR response.

*The UPR triggers IFN production in SKIV2L-depleted cells*

We considered the potential existence of endogenous immunostimulatory RNAs that could trigger the RLRs upon accumulation within cells. We hypothesized that the UPR might provide a source of such RNAs. The UPR is a stress response that is activated when the burden of newly synthesized polypeptides in the endoplasmic reticulum (ER) exceeds its protein folding capacity[25]. UPR activation induces the expression of genes that encode ER protein chaperones, ER membrane biosynthetic enzymes, and the ER-associated protein degradation machinery, thus restoring homeostasis by increasing the size and functional capacity of the ER[28]. One key component of the UPR is the ER-resident, transmembrane kinase/endoribonuclease IRE-1 (refs. [76,77]). The ER luminal domain of IRE-1 is activated directly by misfolded proteins[78,79], leading to the activation of its cytosolic RNA endonuclease domain. The primary role or IRE-1 in UPR induction is to catalyze the removal of a small intron from the mRNA encoding the XBP1 transcription factor by precisely cleaving the XBP1 mRNA at each end of the intron (**Fig. 2.2a**, [27,80]). The resulting exons are then spliced by tRNA ligase[81], and this newly spliced mRNA encodes functional XBP1 protein, which migrates to the nucleus and induces the expression of dozens of UPR-inducible genes[25]. In addition to its role in XBP1 mRNA splicing, IRE-1 in metazoan organisms also mediates the destructive cleavage of many ER-localized mRNAs (**Fig. 2.2a**;[32,82]). This regulated IRE-1-dependent RNA decay (RIDD) transiently reduces the burden of newly synthesized proteins entering the ER, protecting it from further proteotoxic stress[32]. IRE-1 endonuclease cleavage generates RNAs with a 3′ cyclic phosphate moiety, and these RNAs are efficiently cleared by the SKI2 RNA exosome[32]. Interestingly, RNAs containing 3′ cyclic phosphates are capable of activating the RLRs[33,83]. Moreover, a recent study found that UPR activation by cholera toxin

triggers an IRE-1-dependent, RIG-I-mediated inflammatory response[84]. Based on these findings, we reasoned that activation of the UPR in SKIV2L-depleted cells might result in an accumulation of endogenous IRE-1 RNA cleavage products that could elicit an ectopic type I IFN response.

We knocked down SKIV2L or XRN1 in immortalized mouse embryonic fibroblasts and then stimulated these cells with thapsigargin, a chemical inhibitor of the sarco/endoplasmic reticulum calcium ATPase (SERCA) that depletes calcium stores from the ER and triggers a potent UPR. Upon induction of the UPR, we found that SKIV2L-depleted cells activated significant IFN-β production that we did not observe in either XRN1-depleted cells or cells transduced with scramble shRNA (**Fig. 2.2b**). We observed a similar induction of IFN-β in SKIV2L-depleted primary BMDMs treated with thapsigargin, but again not in control or XRN1-depleted macrophages (**Fig. 2.2c**). To extend these findings, we treated BMDMs with tunicamycin, a nucleoside antibiotic that inhibits N-linked glycosylation and induces the UPR by causing the accumulation of unglycosylated proteins in the ER[25]. We treated macrophages with thapsigargin or tunicamycin and monitored the kinetics of UPR activation by tracking the IRE-1-dependent splicing of XBP1 mRNA[85]. We found that thapsigargin-induced XBP1 mRNA splicing was nearly complete at two hours post treatment and returned to baseline by 24 hours (**Fig. 2.2d**). In contrast, tunicamycin-induced XBP1 mRNA splicing occurred with delayed kinetics, commencing at 6 hours and continuing through 24 hours (**Fig. 2.2d**). Interestingly, both thapsigargin and tunicamycin activated IFN-β production in SKIV2L-depleted cells with kinetics that precisely mirrored activation of IRE-1 (**Fig. 2.2e,f**). Thus, two mechanistically distinct activators of the UPR trigger a substantial antiviral response in SKIV2L-depleted cells.

*SKIV2L-deficient humans have a type I IFN signature*

We next explored a role for SKIV2L in regulating the type I IFN response in humans. Loss-of-function mutations in the human *SKIV2L* gene cause tricohepatoenteric syndrome (THES; OMIM 222470; ref. [38]). THES is an extremely rare disease characterized by growth retardation, facial dysmorphism, immunodeficiency, liver and intestine abnormalities and intractable diarrhea that requires parenteral nutrition[39]. These severe symptoms likely reflect the broad role for the cytosolic RNA exosome in maintaining RNA homeostasis within cells, as discussed below. In addition to the mutations in *SKIV2L*

that cause THES, loss-of function mutations in *TTC37*, the human ortholog of the yeast SKI3 RNA exosome component, also cause the same disease[36,37].

We obtained peripheral blood samples from two of the four living THES patients with biallelic *SKIV2L* mutations, as well as from three THES patients with *TTC37* mutations and three controls heterozygous for THES mutations (**Table 2.1**). We confirmed complete loss of SKIV2L protein in extracts derived from a lymphoblastoid cell line derived from a THES patient with biallelic *SKIV2L* mutations (**Fig. 2.4a**), providing further support for the notion that these *SKIV2L* mutations are indeed loss-of-function. We measured the relative abundance of six IFN-stimulated genes (ISGs) by quantitative RT-PCR using cDNA prepared from fresh blood samples: *IFI27, IFI44L, IFIT1, ISG15, RSAD2, and SIGLEC1*. To establish the range of ISG expression in a well-characterized, IFN-mediated human autoimmune disorder and for comparison with our THES samples, we reproduced the recently published ISG profiles of blood samples from 82 AGS patients and 29 healthy controls, adding three additional controls of individuals heterozygous for THES mutations (**Fig. 2.4b**;[86]). Remarkably, we found that both of the SKIV2L-deficient THES patients had a type I IFN signature that was even more robust than the mean ISG scores in AGS patients (**Fig. 2.4b,c**). In contrast, we found no evidence for an IFN signature in the three THES patients with *TTC37* mutations (**Fig. 2.4b,c**). Our findings reveal a strong IFN signature in SKIV2L-deficient THES patients, establishing an important role for SKIV2L in the negative regulation of the IFN-mediated antiviral response in humans. However, the lack of IFN signature in TTC37-deficient THES patients raised the possibility that SKIV2L and TTC37 contribute differently to this negative regulation.

*Differential roles of SKIV2L and TTC37 RLR regulation*

Based on the presence of an IFN signature in SKIV2L-deficient THES patients and its absence in TTC37-deficient patients with the same disease, we wondered whether SKIV2L has a unique function in RLR regulation that is distinct from its role in the classical cytosolic RNA exosome defined by both SKIV2L and TTC37. We therefore established stable and efficient lentiviral knockdown of TTC37 in primary murine macrophages (**Fig. 2.5a**). We found that SKIV2L depletion markedly enhanced the IFN response to transfected RLR ligands. In contrast, TTC37-depleted macrophages exhibited an IFN response that was similar to control cells (**Fig. 2.5b**). Similarly, SKIV2L knockdown enhanced the IFN

response to thapsigargin-induced UPR activation, but TTC37 knockdown had no effect (**Fig. 2.5c**). Together with the THES patient ISG data presented in **Fig. 2.4**, these findings reveal that SKIV2L plays a unique role in the regulation of RLR responses that is distinct from its role in the SKIV2L-TTC37 cytosolic RNA exosome.

**Discussion**

Our data extend the paradigm of negative regulation of cell-intrinsic innate antiviral responses that was first described for the DNA sensing pathway[5] by identifying a key negative regulator of the RLRs that detect RNA. We find that the cytosolic RNA exosome, defined by the SKIV2L RNA helicase, is important for limiting the activation of RLRs. We identify the UPR as a cellular stress response that generates endogenous RLR ligands, and we show that cells undergoing a UPR trigger an aberrant IFN-mediated antiviral response if these endogenous RNAs fail to be metabolized. We show that humans with SKIV2L deficiency have a strong type I IFN signature in their peripheral blood, indicative of a chronic antiviral response that may be relevant to human autoimmune disorders. Finally, we present evidence in human patients and in mouse cells that the role of SKIV2L in RLR regulation is independent of another exosome protein, TTC37. Taken together, these findings reveal a new mechanism of RLR regulation and emphasize the importance of intracellular nucleic acid metabolism for preventing aberrant innate immune responses.

We found that SKIV2L-depleted cells, but not XRN1-depleted cells, had a massively enhanced IFN-$\beta$ response to RLR ligands. Perhaps more relevant to autoimmune disease, we identify the RNA degradation products of IRE-1 that are generated during the UPR as a source of endogenous immunostimulatory RNAs that trigger a MAVS-dependent IFN response in SKIV2L-depleted cells, but not in wild-type cells. Importantly, this finding reveals a mechanism by which a "sterile" stress response could be misinterpreted as a viral infection if cells fail to metabolize the RNA degradation products that are formed as a result of the stress. The UPR-activated RLR response in SKIV2L-depleted cells was robust and significant, but much less potent than the response to transfected triphosphate RNAs. This likely reflects the number of RIG-I ligands introduced by transfection: one microgram of transfected RIG-I ligand contains approximately $10^{13}$ molecules, which would amount to ~10 million molecules delivered per cell in our experimental system. In contrast, IRE-1-mediated cleavage of cellular mRNAs would generate far fewer endogenous RIG-I ligands. Moreover, it is also likely that 3′ cyclic phosphate RNAs are less efficient activators of RLRs than 5′ triphosphate RNAs[33,84]. Despite the relatively weaker

IFN response triggered by the UPR, we propose that such an IFN response in a chronic setting would be sufficient to drive substantial pathology.

Our findings suggest a new potential mechanism for the pathogenesis of certain autoimmune diseases that affect highly secretory cells that routinely undergo ER stress, including Sjögren's syndrome (which affects salivary and lacrimal glands) and Type I diabetes (which affects insulin-secreting $\beta$ cells of the exocrine pancreas). We propose a simple model in which regular, episodic activation of the UPR would generate endogenous RIG-I ligands. In individuals with deficiencies in their ability to metabolize these RNAs, this UPR would trigger a chronic, inappropriate antiviral response, leading to immune activation and eventual destruction of the cells over time. Importantly, our model emphasizes the role of the secretory cells themselves as active participants in the autoimmune process. By activating the cell-intrinsic antiviral response, these cells become the targets of an adaptive immune response, similar to the manner in which virus-infected cells are targeted for elimination by cytotoxic T cells.

We show that human patients with SKIV2L deficiency have a potent IFN signature in their peripheral blood cells, thus providing important evidence for the relevance of this regulatory mechanism to human disease. Our findings raise two important questions. First, does this IFN signature contribute to the pathogenesis of THES? Based on the lack of IFN signature in TTC37-deficient THES patients, we propose that most of the symptoms of this severe disease are the consequence of loss of the 'housekeeping' function of the cytosolic RNA exosome in general RNA turnover, rather than the aberrant IFN response that is found only in SKIV2L-deficient patients. Second, given the strong IFN signature, why do SKIV2L-deficient patients not develop autoimmunity? Interestingly, some THES patients also exhibit immunodeficiency and require supplemental immunoglobulins[39], suggesting an essential role for the RNA exosome in lymphocyte function. Indeed, we found that the survival of our SKIV2L-knockdown cells was compromised after stimulation, precluding a number of experiments that we attempted to perform, including RNA virus infections (data not shown). Taken together, we suggest that defective lymphocyte function in THES patients prevents overt autoimmune disease, despite the potent IFN signature evident in their peripheral blood cells. However, the immunological aspects of

THES have thus far been incompletely defined, in large part because of the extreme rarity of the disease and the severity of the other symptoms. It will be informative to further explore potential autoimmune phenotypes in THES and their differential manifestation in patients with SKIV2L mutations and TTC37 mutations, in light of the findings presented above.

We present evidence that SKIV2L contributes to RLR regulation, but the other defined component of the cytosolic RNA exosome, TTC37, does not. The subcellular localization and RNA substrate specificity of the RNA exosome is determined by its associated cofactors, such that the exosome associated with SKIV2L and TTC37 is primarily involved in cytosolic RNA decay[22]. Moreover, the RNA exonucleases that also associate with the core exosome components can each mediate degradation of unique subsets of RNAs within cells[22]. We propose that the role for SKIV2L uncovered here is distinct from its involvement in the conventional cytosolic RNA exosome, and it will be interesting to determine whether there are proteins that partner with SKIV2L that are uniquely involved in RLR regulation. Such proteins may serve to target SKIV2L specifically to immunostimulatory RNAs.

In summary, we identify a regulatory mechanism in which metabolism of intracellular RNA ligands limits activation of the RIG-I-like receptors. We propose that deficient function of this regulatory mechanism would predispose to autoimmune diseases, particularly those that affect highly secretory cells. Identification of other components of this pathway may provide insight into the pathogenesis of certain IFN-associated autoimmune disorders.

# Chapter 3 Figures

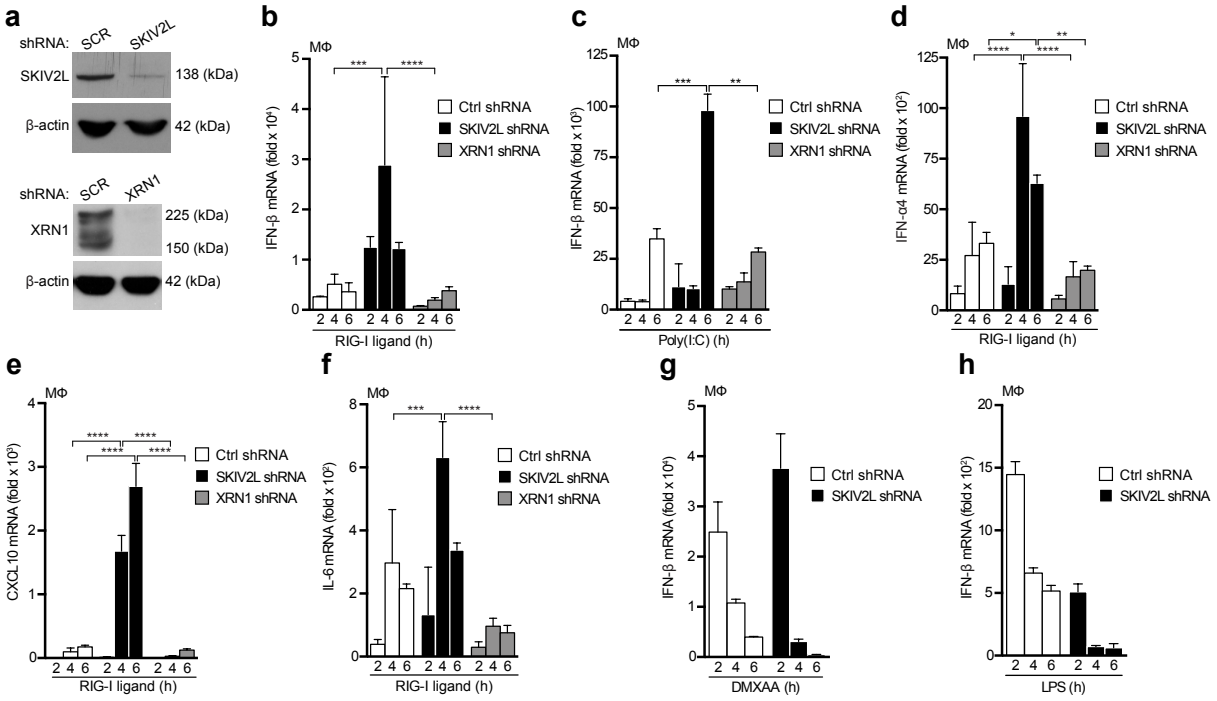


*Figure 2.1: SKIV2L is a negative regulator of the RIG-I-like receptor-mediated antiviral response.*

**(a)** SKIV2L and XRN1 were stably knocked down in primary macrophages, and the respective protein levels were evaluated by western blotting.

**(b-c)** Primary mouse macrophages, stably transduced as indicated with shRNA knockdown constructs, were treated with an HCV RIG-I ligand (**b**) or Poly (I:C) (**c**) and assessed for IFN-ß production by quantitative RT-PCR.

**(d-f)** RIG-I ligand-stimulated macrophages with the indicated knockdown constructs were evaluated by quantitative RT-PCR for expression of IFNa4 (**d**), CXCL10 (**e**) and IL-6 (**f**).

**(g-h)** Macrophages were stimulated with DMXAA to activate STING directly, and with LPS to activate TLR4. **P* < 0.05; ***P* < 0.001; ****P* < 0.0005; *****P* < 0.0001 (2way ANOVA, **b-f**). Data are representative of at least three independent experiments with biological triplicates (mean + s.d., **a-h**).

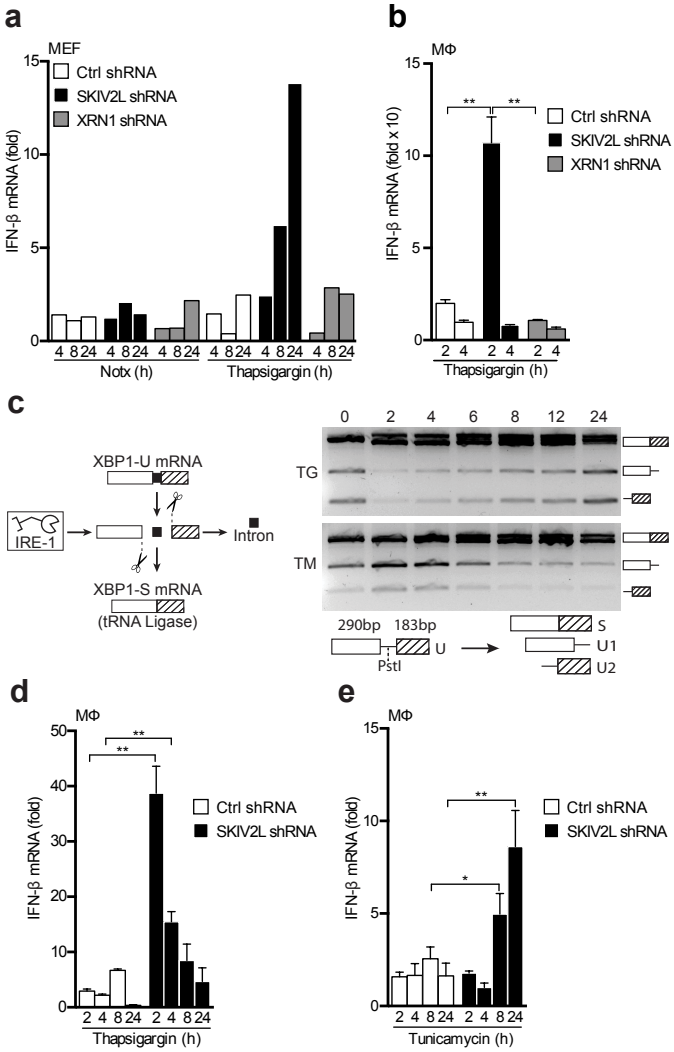


*Figure 2.2: The UPR activates an antiviral response in SKIV2L-depleted cells.*

**(a)** SV40 Large T antigen-immortalized mouse embryonic fibroblasts were transduced with the indicated knockdown constructs and treated with thapsigargin (TG). *Ifnb* mRNA induction was evaluated using quantitative RT-PCR at the indicated time points. Data are representative of 3 experiments.

**(b)** Primary mouse macrophages were transduced and treated as in (**a**).

**(c)** Endonuclease activity of IRE-1 is responsible for removal of an intron in XBP-1 mRNA, as well as destructive cleavage of ER-localized RNAs. The kinetics of UPR activation were assessed using a splicing assay for XBP-1 mRNA. The illustration shows the PstI digest site in the intron of unspliced XBP-1 mRNA used to distinguish spliced (S) and unspliced (U1, U2) cDNAs.

**(d-e)** Primary mouse macrophages were treated with thapsigargin (TG; **e**) or tunicamycin (TM; **f**) treatment. **P* < 0.05; ***P* < 0.0001 (2way ANOVA, **b-e**). Data are representative of at least three independent experiments with biological triplicates (mean + s.d., **b-e**).

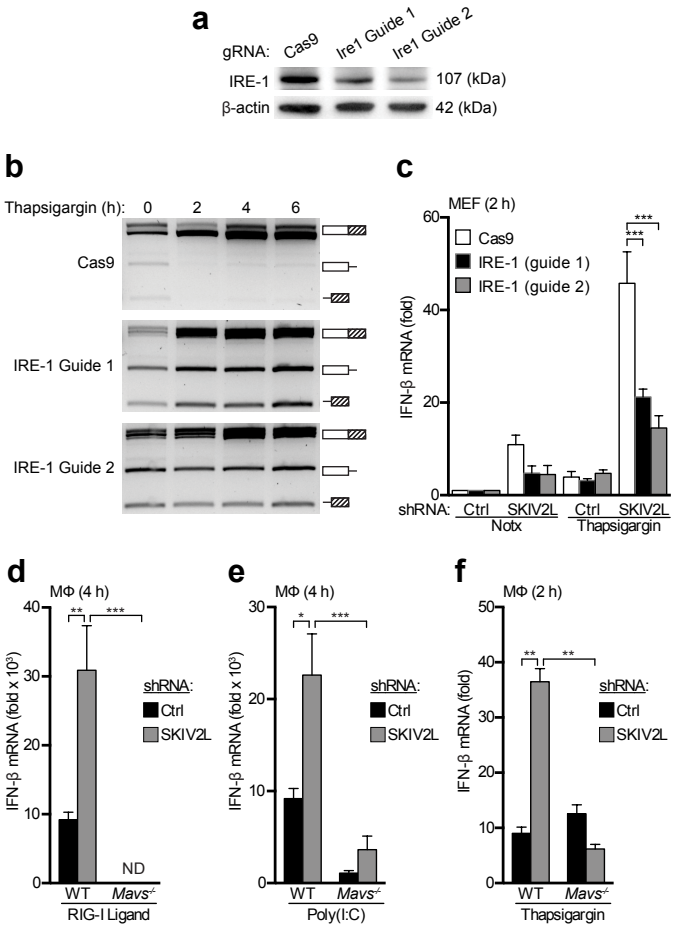


*Figure 2.3: SKIV2L specifically regulates the MAVS-dependent antiviral response.*

**(a)** Immortalized MEFs were transduced with lenti-CRISPR constructs encoding CAS9 alone or two different guide RNAs targeting *Ern1*. IRE-1α protein was measured by western blot.

**(b)** CAS9 control and IRE-1α-targeted cells were treated with thapsigargin to induce the UPR, and IRE-1- mediated XBP-1 mRNA splicing was quantitated as in Fig. 2d.

**(c)** Control and IRE-1-targeted cells were treated with thapsigargin, and IFN-β mRNA was measured by quantitative RT-PCR at the indicated time points. Data are representative of one experiment with biological triplicates testing two independent guide RNAs (mean + s.d., **a-c**).

**(d-f)** Bone marrow macrophages of the indicated genotypes were transduced with a control or SKIV2L shRNA, treated with RIG-I ligand (**d**), Poly I:C (**e**), or thapsigargin (**f**), and harvested for analysis at the indicated time points. **P* < 0.001; ***P* < 0.0005; ****P* < 0.0001; (2way ANOVA, **c-f**). Data are representative of at least three independent experiments with biological triplicates (mean + s.d., **d-f**).

**Table 2.1**

| Status | Gene Mutated | Mutation 1 | Mutation 2 | Protein | Gender | Age at Harvest | Ancestry | Consanguinity |
|---|---|---|---|---|---|---|---|---|
| Control | SKIV2L | c.1635insA | - | p.Gly546Argfs*35 | Male | 49 | North Africa | - |
| Control | SKIV2L | c.1635insA | - | p.Gly546Argfs*35 | Female | 43 | North Africa | - |
| Control | TTC37 | c.3960C>A | - | p.(Tyr1320*) | Male | 50 | North Africa | - |
| THES | SKIV2L | c.3561_3581del | c.3561_3581del | p.(Ser1189_Leu1195del) | Male | 1 | Kuwait | Yes |
| THES | SKIV2L | c.848G>A | c.1022T>G | p.(Trp283*), p.Val341Gly | Female | 4 | France | No |
| THES | TTC37 | c.3960C>A | c.3960C>A | p.(Tyr1320*) | Male | 10 | France | Yes |
| THES | TTC37 | c.2808G>A | c.2808G>A | p.Trp936* | Male | 5 | Pakistan | Yes |
| THES | TTC37 | c.2779-2G>A | c.2779-2G>A | p.Glu974Glyfs*19 | Male | 9 | Pakistan | Yes |

*Table 2.1: Details of ancestry and mutations in THES peripheral blood samples*

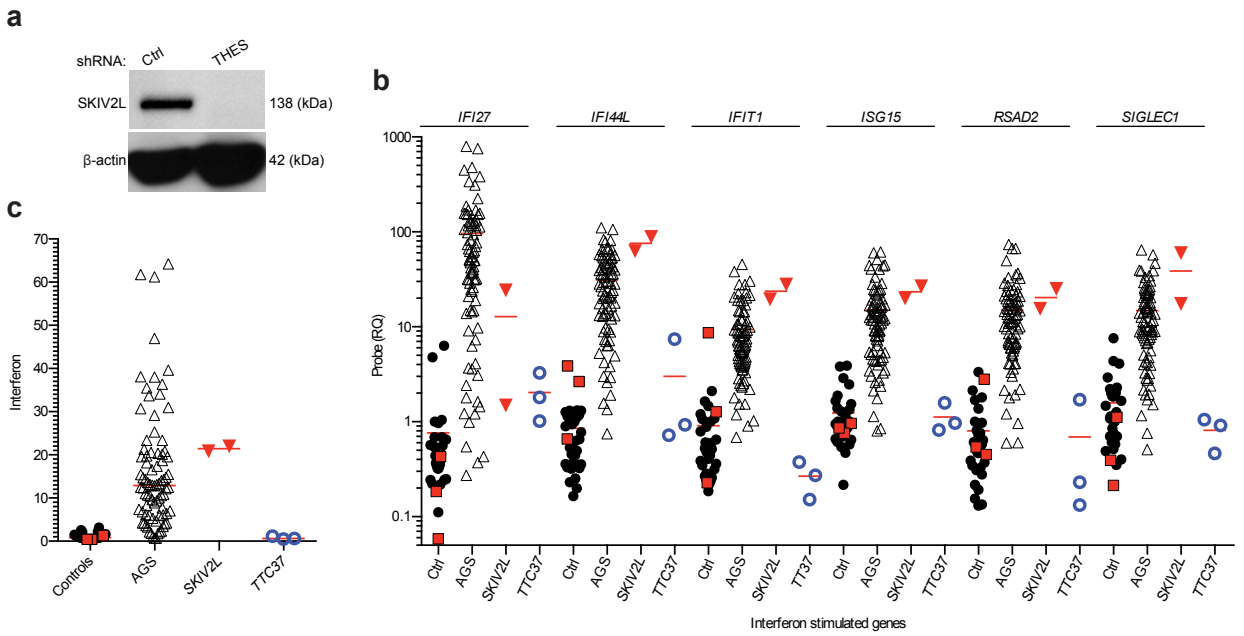


*Figure 2.4: SKIV2L-deficient humans have a robust type I IFN signature.*

**a)** SKIV2L protein levels were evaluated by western blot in control and THES (c.1635insA/c.1635insA) patient lymphoblastoid cell lines.

**(b)** Quantitative RT-PCR measuring six human interferon-stimulated genes (ISGs) in cDNA prepared from whole blood. For each gene, we present values from 29 AGS control patients (black closed circles) together with 3 controls with heterozygous THES mutations (red filled squares), 82 AGS patients (black open triangles), 2 THES patients with *SKIV2L* mutations (red filled triangles), and 3 THES patients with *TTC37* mutations (blue open circles). Horizontal bars represent the median relative quantification (RQ) value for each ISG probe in each group, normalized to *HPRT* and 18S rRNA expression within each sample. Note that the data from AGS controls and AGS patients were recently published[44] and are reproduced here for comparison to the THES controls and THES patients.

**(c)** Interferon scores were calculated using the median fold change in RQ value for all of the six interferon-stimulated genes in each individual as described[44]. Horizontal bars show the mean interferon scores in patients and controls.

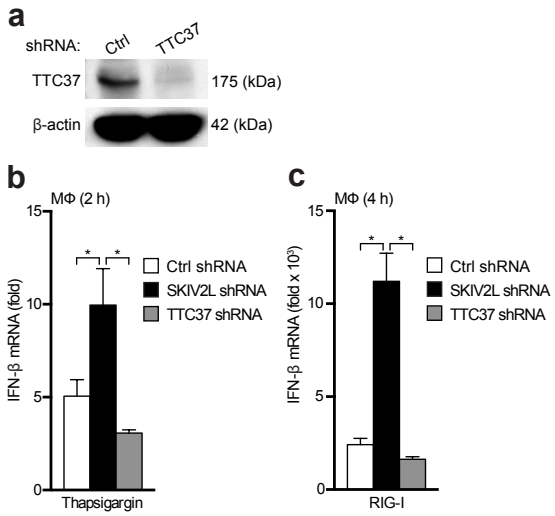


*Figure 2.5: Differential role of SKIV2L and TTC37 in RLR regulation.*

**(a)** Western blots of primary BMDM lysates showing TTC37 expression in knockdown and control cells.
**(b-c)** Cells were transduced with the indicated lentiviral shRNA constructs and treated with the indicated ligands. **P* < 0.01; ***P* < 0.005; ****P* < 0.0001; (one-way ANOVA, **b-c**). Data are representative of two independent experiments with biological triplicates (mean + s.d., **a-c**).

**Table 2.2**

| Construct/Oligo | 5'-3' Sequence |
|---|---|
| **PU/UC A** | AAAGGAAAGAAAAGGAAAAAAAGAGGAAAAAAAAAGGAGAAAAAAAAAAAAAAAAAAAAAA<br>AAAAAAAAAAAGAAAAAAAAAAAGGGAAAAAAACAGGATGGCCTATAGTGAGTCGTATTA |
| **Murine IFNb S** | GCACTGGGTGGAATGAGACTATTG |
| **Murine IFNb AS** | TTCTGAGGCATCAACTGACAGGTC |
| **Murine CXCL10 S** | AAGTGCTGCCGTCATTTTCTGCCTC |
| **Murine CXCL10 AS** | CTTGATGGTCTTAGATTCCGGATTC |
| **Murine IL-6 S** | GACTTCCATCCAGTTGCCTTCTTGG |
| **Murine IL-6 AS** | CCAGTTTGGTAGCATCCATCATTTCT |
| **Murine HPRT S** | GTTGGATACAGGCCAGACTTTGTTG |
| **Murine HPRT AS** | GAGGGTAGGCTGGCCTATAGGCT |
| **Murine XBP1.3S** | AAACAGAGTAGCAGCGCAGACTGC |
| **Murine XBP1.2AS** | GGATCTCTAAAACTAGAGGCTTGGTG |
| **mIRE-1 RFLP S** | AGAACTTAGGCCCTCCAACC |
| **mIRE-1 RFLP AS** | GGAGTGCAAGTCCGTTTCCT |
| | *Underlined = T7 minimal promoter* |
| **Human Gene** | **TaqMan Probe Set; Life Technologies** |
| **IFI27** | Hs01086370_m1 |
| **IFI44L** | Hs00199115_m1 |
| **IFIT1** | Hs00356631_g1 |
| **ISG15** | Hs00192713_m1 |
| **RSAD2** | Hs01057264_m1 |
| **SIGLEC1** | Hs00988063_m1 |
| **HPRT1** | Hs03929096_g1 |
| **18S** | Hs999999001_s1 |

*Table 2.2: Primer and TaqMan Sets*

# Chapter 3: RNase L Inactivates Ribosomes to Limit the RIG-I-like Receptor Antiviral Response

**Abstract**

Intracellular detection of foreign DNA or RNA triggers distinct sensors and signaling pathways that protect against viral infection: DNA activates the cyclic GMP-AMP synthase (cGAS)-STING pathway, whereas RNA activates the RIG-I-like receptor (RLR)-MAVS pathway. In addition, the oligoadenylate synthetase (OAS) enzymes detect foreign RNA and catalyze the formation of 2'-5'-linked oligoadenylates (2-5A). The sole known biological function of 2-5A is to activate the endoribonuclease RNase L, which is thought to cleave cellular and viral RNAs indiscriminately into small fragments that are endogenous ligands for the RLRs. We show here that, contrary to this prevailing view, RNase L-deficient cells have an enhanced antiviral response to RLR ligands. We demonstrate that the in vivo specificity of RNase L is restricted to several unique sites in ribosomal RNA (rRNA), and that RNase L activation leads to depletion of translating ribosomes, thus limiting the production of antiviral cytokines. Moreover, we demonstrate that 2-5A molecules are endogenous activators of STING. These findings offer a revised view of RNase L as a specific regulator of protein translation and reveal a new class of endogenous immunostimulatory molecules that link RNA detection by OAS enzymes to activation of the STING pathway.

**Introduction**

RNase L is an endoribonuclease that is important for immunity to RNA viruses. Upon viral infection, RNase L is activated by the 2'-5'-linked oligoadenylate (2-5A) products of the oligoadenylate synthetase (OAS) enzymes[87,88]. The current model of the OAS-RNase L system is that the sole biological function of 2-5A is to bind to and activate RNase L, which then indiscriminately cleaves cellular and viral RNAs into small fragments that act as ligands for the RIG-I-like receptors (RLRs)[33,89]. Thus, RNase L is thought to be an essential positive regulator of the RLR response through its non-specific RNA endonuclease activity. We show here that, contrary to the prevailing view, RNase L-deficient cells have an enhanced antiviral response to RLR ligands. Moreover, we show that 2-5A molecules are endogenous RLR ligands that are most potent in RNase L-deficient cells. Using deep sequencing of RNase L-dependent RNA cleavage products recovered from live cells, we find that its *in vivo* endonuclease specificity is exclusively targeted to several unique sites in ribosomal RNA (rRNA). We find that RNase L can target intact, active ribosomes, resulting in a depletion of translating ribosomes. We propose that the primary function of RNase L is to inactivate ribosomes, which prevents viral replication but also limits production of antiviral cytokines.

Three forms of OAS proteins exist in humans. OAS1 and OAS2 both have two isoforms generated by differential splicing of the same gene, while OAS3 has a single isoform. All three OAS proteins are interferon inducible, but there are unique factors regulating the expression and catalytic activity of each[90]. Catalytic activity of an OAS protein is initiated after binding of double stranded RNA (dsRNA), at which point the enzyme converts ATP into 2'-5'-linked oligomers of differing lengths with a 5'-triphosphate. While this activity was first described over 30 years ago, there have been no functional studies to date evaluating the biological role of the different 2-5A species generated by each OAS protein. When evaluating HPLC-purified 2-5A species containing two to five adenosines, we revealed that transfected dinucleotide functions in an RNase L-independent manner to induce interferon in primary macrophages. Furthermore, and in addition to our observations that 2-5A molecules are RLR ligands, we show that all of these 2-5A species have a STING dependence.

This revised view of the OAS-2-5A-RNase L system has implications for our understanding of its function, substrate specificity, and role in antiviral responses.

**Results**

Activation of RNase L by the 2-5A oligoadenylate products of the OAS enzymes is a well-known component of the antiviral response to infection with RNA viruses[88,91]. The importance of the OAS-RNase L pathway is perhaps best illustrated by the fact that numerous RNA viruses encode antagonists that either prevent OAS activation or degrade 2-5A[92,93]. Additionally, the human *RNASEL* gene was identified as the Hereditary Prostate Cancer Locus 1 (HPC1)[44,45].

We generated primary bone marrow-derived macrophages from wild-type (WT) and RNase L-deficient mice to explore their responses to immunostimulatory nucleic acids. Contrary to a published report[33], we found that transfection of RNase L-deficient cells with a triphosphate RNA ligand for RIG-I resulted in a massively enhanced antiviral response, measured by quantitative RT-PCR of interferon-$\beta$ (IFN$\beta$) mRNA levels. Similarly, transfection of the synthetic RNA ligand Poly I:C led to enhanced responses in RNase L-deficient cells (**Fig. 3.1a**). Infection of *Rnasel-/-* macrophages with vesicular stomatitis virus (VSV) or Sendai virus revealed an equivalent IFN response compared to WT cells, despite a significant increase in VSV titers in the knockout cells several hours after infection (**Fig. 3.2a-b**). Perhaps most surprisingly, we found that purified 2-5A stimulated a potent type I IFN response in RNase L-deficient cells that was over two orders of magnitude stronger than the mild induction seen in wild-type cells (**Fig. 3.1b**). We validated these findings by measuring secreted type I IFN protein in the supernatants of stimulated macrophages, finding enhanced IFN protein production in RNase L-deficient cells stimulated with RIG-I ligand, Poly I:C, or 2-5A (**Fig. 3.1c-d**). This enhanced antiviral response was specific for RLR ligands and 2-5A, because WT and RNase L-deficient macrophages responded identically to transfected DNA (that activates the STING-IFN pathway[63,94]), and lipopolysaccharide (LPS, that activates TLR4-TRIF[75]; **Fig. 3.1a, c**).

We next derived primary murine embryonic fibroblasts (MEFs) from WT and RNase L-deficient mice, and we again found enhanced IFN responses to RIG-I ligand and 2-5A, but not to transfected DNA (**Fig. 3.1e, f**). To evaluate the scope of the enhanced response in RNase L-deficient cells, we performed cDNA microarray analysis on RNAs harvested from macrophages four hours after stimulation with RIG-I ligand, 2-5A, or DNA. We plotted the relative mRNA levels of over 11,000 expressed genes,

comparing their induction in WT and RNase L-deficient cells. Transfection with DNA, which does not activate RNase L (**Fig. 3.2c**), resulted in a nearly identical induction of antiviral genes in WT and RNase L KO macrophages (**Fig. 3.1g**). In contrast, treatment with RIG-I ligand or 2-5A revealed hundreds of genes with enhanced induction in RNase L-deficient cells (**Fig. 3.1g**). These genes were highly enriched for type I IFNs and IFN-stimulated genes (ISGs), consistent with a broad effect of RNase L-deficiency on the inducible antiviral response (**Fig. 3.1h**). We also identified a class of RNase L-dependent genes that was induced only in WT cells by RIG-I ligand and 2-5A and not by DNA transfection (**Fig. 3.1g and Fig. 3.3**).

We were particularly interested in the antiviral response triggered by direct transfection of 2-5A into RNase L-deficient cells because the sole known function of 2-5A is to activate RNase L[95,96]. We found that this IFN response to 2-5A was significantly abrogated in *Rnasel-/- Mavs-/-* cells that lack RLR-induced antiviral responses[97] (**Fig. 3.3a**). Similarly, the responses to RIG-I ligand in both WT and *Rnasel-/-* macrophages required MAVS (**Fig. 3.3e**). In contrast, neither RNase L deficiency nor MAVS deficiency influenced the antiviral responses to DNA transfection or LPS stimulation (**Fig. 3.3e**). To test whether 2-5A itself is a RLR ligand, we used micrococcal nuclease (MN), which hydrolyzes 3'-5' phosphodiester bonds in RNA and DNA, but largely spares the 2'-5' bonds in 2-5A[87]. We found that the IFN response to both RIG-I ligand and DNA was sensitive to pre-treatment with MN, but the response to 2-5A was not (**Fig. 3.3b**). Next, we treated cells with HPLC-purified dimers, trimers, tetramers, and pentamers of 2-5A[58]. The trimer, tetramer, and pentamer species of purified 2-5A stimulated IFN protein production in RNase L-deficient macrophages but not in WT cells (**Fig. 3.3c and Extended Data Fig. 3.2**), and they activated rRNA cleavage in WT cells but not RNase L-deficient cells (**Fig. 3.3d**). Remarkably, the dimer of 2-5A, which is incapable of activating RNase L and is thought to be an inert intermediate in the synthesis of larger 2-5A forms[87] (**Fig. 3.3d**), triggered IFN production in both WT and *Rnasel-/-* cells (**Fig. 3.3c**). Together, these findings demonstrate that pure 2-5A species are endogenous RLR ligands. Moreover, the novel activity of the 2-5A dimer described here may provide a reason for the existence of the mammalian OAS3 enzyme, which preferentially synthesizes only 2-5A dimers[98].

To explore the mechanism of RNase L-dependent regulation of the RLR response, we prepared libraries of RNase L-dependent RNA cleavage products harvested from live cells four hours after activation by RIG-I ligand or 2-5A. RNase L cleavage leaves cyclic phosphates on the 3' termini of cleaved RNAs. We exploited this feature of RNase L chemistry by using purified tRNA ligase to ligate RNA oligonucleotide adapters containing 5' hydroxyl moieties to the 3' phosphate-containing RNAs [99]. These 5'-OH adapters each contained a unique molecular identifier (UMI) to allow the precise quantitation of ligation events[100,101]. By comparing UMI-corrected, 3' phosphate RNA libraries prepared from stimulated and untreated cells of both WT and *Rnasel-/-* mice, we identified inducible, RNase L-dependent endonucleolytic events in RNAs recovered from live cells (**Extended Data Figs. 3.4-3.13 and Tables 1-12**).

Much of what is known about RNase L specificity is based on experiments in which purified RNase L is mixed *in vitro* with 2-5A and extracted RNAs. Under these non-physiological conditions, RNase L indiscriminately cleaves mRNAs, rRNAs, tRNAs, and viral RNAs, with a preferred cleavage site located between nucleotides at positions +1 and +2 following a uracil (UX^X;[102]). We were therefore surprised to find that the *in vivo* specificity of RNase L is exclusively directed towards rRNA, with no evidence of RNase L-dependent cleavage sites in any other cellular RNAs (**Fig. 3.4a and Extended Data Tables 1-12**). RNase L-mediated cleavage of rRNA occurred at several specific sites, only in WT cells, and only after stimulation with RIG-I ligand or 2-5A, as shown by mapping of 3' phosphate RNAs along 18S rRNA (**Fig. 3.4b**) and 28S rRNA (**Fig. 3.4c**), as well as by comparing unique reads recovered from WT and RNase L-deficient cells (**Fig. 3.4d**). We mapped these rRNA cleavage sites to the recently solved crystal structure of the complete human ribosome[103], revealing that RNase L targets a broad patch of rRNA in the ribosome while sparing numerous other exposed regions of rRNA (**Fig. 3.4e**), suggesting specific recruitment of RNase L to this region of the ribosome. A recent study found similar rRNA cleavage sites human cells[100], including an identical site in 18S rRNA targeted by both human and murine RNase L (**Fig. 3.4e**). Fragmentation of rRNA has long been used as an indicator of RNase L activity[104,105], thought to reflect its indiscriminate targeting of cellular RNAs. Our data, however, suggest that rRNA may be the *only* relevant target of RNase L *in vivo*. It is possible that mRNAs or other

cellular RNAs are cleaved by RNase L at levels below the detection threshold of this assay[106]. However, we found no mRNAs with expression levels that were reduced in an RNase L-dependent manner in our microarray analyses (**Fig. 3.1g**). Similarly, a recent study found that extracted polio virus RNA is extensively degraded by RNase L *in vitro*, but is cleaved at only a single site by RNase L during polio infection of live cells[100]. Thus, the *in vivo* specificity of RNase L is highly constrained relative to its activity in a test tube.

We next analyzed the consequences of RNase L activation on ribosome function. We performed polyribosome sedimentation using immortalized murine fibroblasts stably expressing epitope-tagged, wild type RNase L or a catalytic mutant (R666A) of RNase L. The distribution of rRNA across the polyribosome gradient in unstimulated MEFs expressing WT RNase L revealed abundant mRNA translation, as measured by the broad peak of RNA present in later fractions and the comparably low levels of free 40S and 60S ribosomal subunits (**Fig. 4.4a**). Treatment of these cells with 2-5A for two hours resulted in a dramatic loss of translating ribosomes, measured by a shift of RNA signal towards the less dense region of the gradient (**Fig. 4.4a**). The distribution of rRNA across the gradients mirrored this shift of RNA signal after treatment with both RIG-I ligand and 2-5A (**Fig. 4.4b**). Interestingly, we detected significant rRNA fragmentation within the translating ribosomes in the dense fractions of the gradient, with the majority of cleaved rRNA appearing in the lighter fractions (**Fig. 4.4b, arrows**). In contrast, cells expressing the catalytically inactive RNase L mutant maintained abundant mRNA translation after stimulation with both of these ligands (**Fig. 4.4b, bottom row**), with no detectable degradation of rRNA. Importantly, we used quantitative, kinetic imaging to demonstrate that these cells were not dying during the timeframe of these experiments (**Extended Data Fig. 3.3**), thus ruling out the possibility of non-specific toxicity as the cause of these dramatic changes in ribosome distribution. We performed similar experiments in primary macrophages and found that wild-type cells exhibited a reduction of translating ribosomes after treatment with RIG-I ligand or 2-5A, but *Rnasel*-/- cells maintained robust levels of polyribosomes (**Fig. 4.4c**). Together, these data demonstrate that the principal role of RNase L is to inactivate ribosomes, consistent with the inhibition of mRNA translation first ascribed to the OAS-RNase L system when its existence was discovered almost 40 years ago[49,87,91].

With our revised model of RNase L and the antiviral response, we decided to gain a better understanding of how the 2-5A dimer was inducing interferon in an RNase L-independent manner. We observed that interferon induction in cells transfected with 2-5A dimer was not diminished at all in *Mavs*$^{-/-}$ mice, but that induction was entirely dependent on STING (**Fig. 4.5a**). Treatment of these cells with RIG-I ligand or calf thymus DNA showed the expected dependence on MAVS and STING, respectively (**Fig. 4.5a**). To evaluate the role of the adaptors MAVS and STING in the absence of RNase L catalytic activity, we pretreated cells with a chemical IRE-1 alpha endonuclease inhibitor, STF. Inhibition was effective due to the considerable nuclease domain homology between IRE-1 and RNase L. Much to our surprise, however, was the fact that MAVS-dependent interferon production following 2-5A transfection was only partial, and complete loss of cytokine production was only observed in *Sting*$^{-/-}$ cells (**Fig. 4.5b**).

**Discussion**

Our findings warrant a revisiting of the model of OAS-RNase L function in antiviral immunity (**Fig. 4.4d**). We propose that there are two reasons for the enhanced RLR response seen in *Rnasel*-/- cells: the inherent immunostimulatory activity of endogenous 2-5A molecules (**Fig. 3.3 and 4.5**), and the increased translation of mRNAs encoding IFNs and ISGs (**Fig. 4.4d**). Similarly, the human *RNASEL* mutations associated with prostate cancer may predispose to tumourigenesis for the same two reasons: enhanced RLR responses activated by 2-5A in *RNASEL* mutant cells may cause chronic inflammation, and failure to control mRNA translation may enable enhanced growth of transformed cells. The identification of 2-5A molecules as both RNase L activators and endogenous RLR ligands suggests that further exploration of the three functional OAS enzymes in humans will yield new insights into the activation of the RLR antiviral response. Interestingly, cyclic GMP-AMP synthase (cGAS), an OAS-related enzyme that generates a 2'-3'-linked cyclic dinucleotide called cGAMP, was recently found to be essential for the antiviral response to intracellular DNA[54,107]. Thus, the OAS enzyme family contributes to the activation of antiviral immunity downstream of both RNA and DNA detection.

The effect of RNase L on mRNA translation must be considered in the context of the other, well established mechanism for restricting mRNA translation during the RNA-activated antiviral response: phosphorylation of the eukaryotic initiation factor 2$\alpha$ (eIF2$\alpha$) by protein kinase R (PKR[108]). Both OAS-RNase L and PKR are activated by the same immunostimulatory RNAs that trigger the RLRs. However, PKR blocks translation at the level of initiation, whereas RNase L blocks translation by inactivating ribosomes. This dual regulation of distinct aspects of mRNA translation raises important questions about their coordination during the antiviral response. How is RNase L recruited to ribosomes, accounting for the specific regions of rRNA that are targeted? Are there cofactors for RNase L that determine its restricted specificity *in vivo*? Are there mRNAs that escape this level of regulation, similar to the manner in which translation of certain mRNAs is enhanced in the presence of phosphorylated eIF2$\alpha$[108]? In the context of the new model of the OAS-RNase L system provided here, addressing these questions will provide important insights into regulation of innate immune responses to RNA viruses.

# Chapter 3 Figures

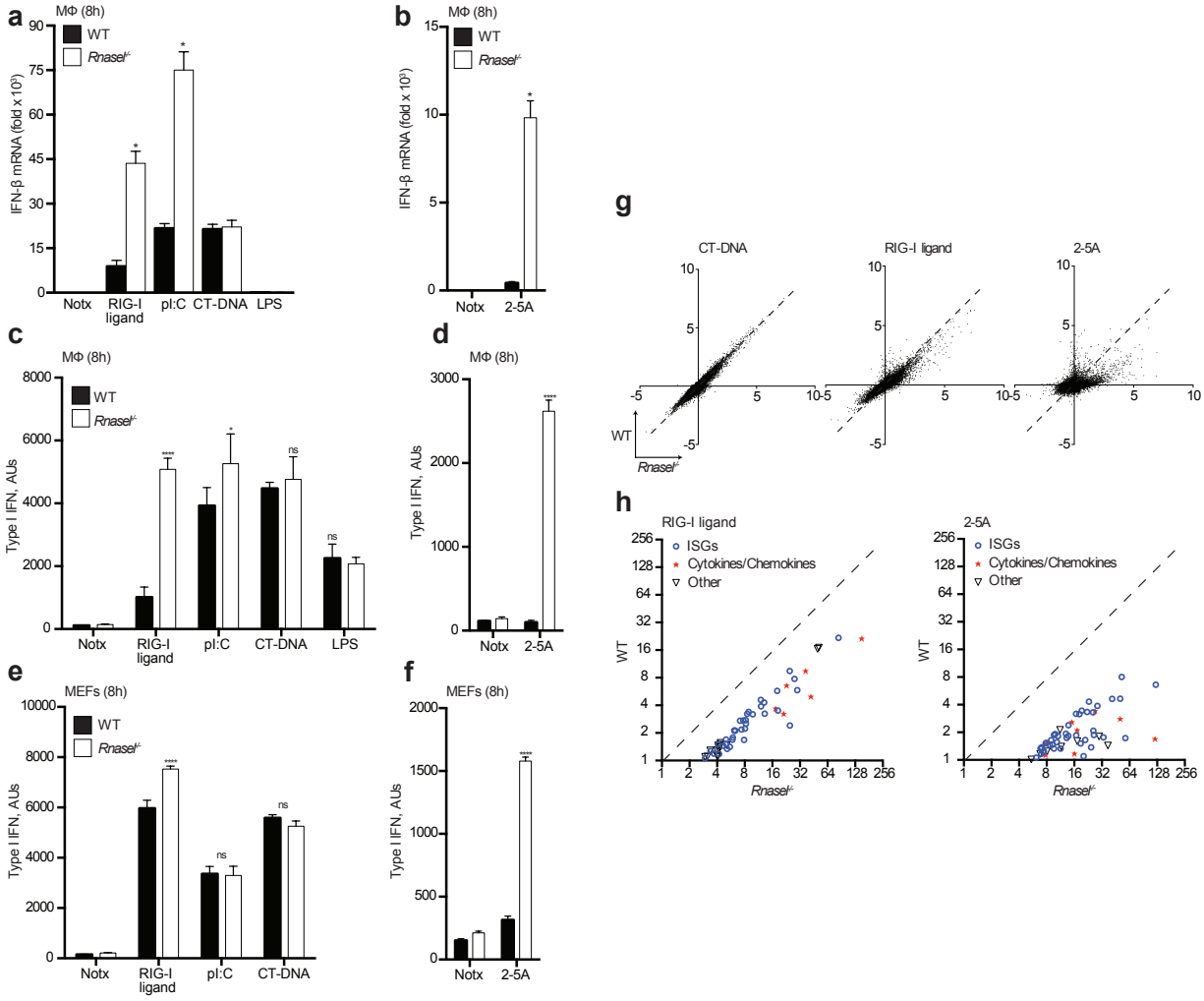


*Figure 3.1: RNase L-deficient cells have an enhanced antiviral response to RLR ligands and 2-5A*

**(a-b)** Bone marrow-derived macrophages of were treated with the indicated ligands for 8 hours, and Ifnb mRNA was measured by quantitative RT-PCR, normalized to Hprt expression, and compared to untreated cells.
**(c-d)** Supernatants from macrophages, treated as above, were evaluated for type I IFN activity using a bioassay.
(**e-f)** Primary MEFs were treated with the indicated ligands for 8 hours, and type I IFN protein was measured in supernatants by bioassay.
(**g)** Primary macrophages were treated with the indicated ligands for six hours, followed by RNA isolation and cDNA microarray analysis. Each dot represents a single mRNA, and expression levels are presented in $\log_2$ format. The dashed line indicates equivalent expression between WT and *Rnasel*$^{-/-}$ cells.

(**h)** The top genes with enhanced expression in *Rnasel*$^{-/-}$ macrophages after treatment were annotated for known ISGs, IFNs and cytokines, or other mRNAs. The dashed line indicates equivalent expression. All data are representative of 2-5 experiments, with biological replicates within each experiment.

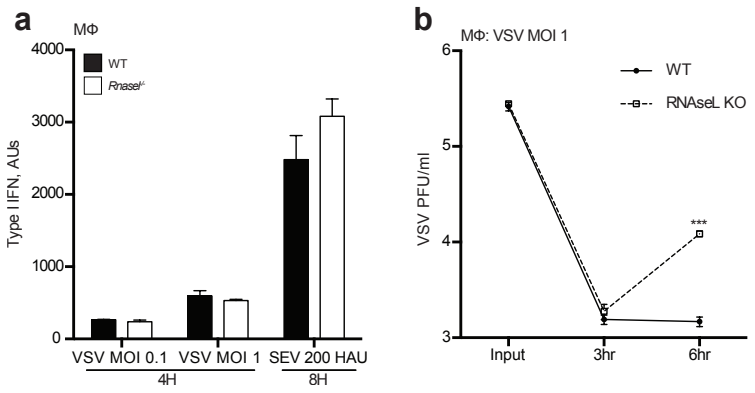


*Figure 3.2: Viral clearance is not dependent on RNase L-dependent interferon induction*

**(a)** Bone marrow-derived macrophages from WT and RNase L deficient mice were infected with VSV or Sendai virus for the indicated times. Supernatants were evaluated for type I IFN activity using a bioassay

**(b)** Macrophages infected as above had VSV titers evaluated by a plaque assay at the times indicated.

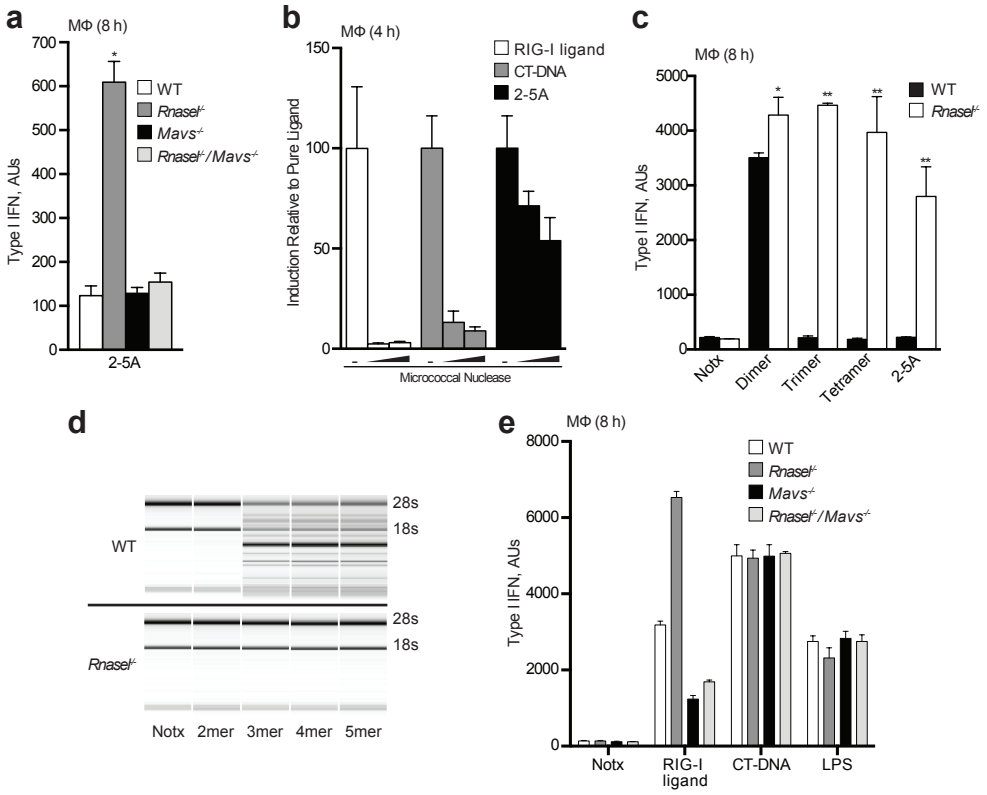


*Figure 3.3: 2-5A molecules are endogenous RLR ligands*

**(a)** Macrophages of the indicated genotypes were stimulated for 8 hours with 2-5A, and type I IFN activity was measured in culture supernatants.

**(b)** The indicated ligands were pretreated with micrococcal nuclease prior to transfection into RNase L-deficient macrophages. Type I IFN activity was measured in culture supernatants harvested 8 hours post treatment.

**(c)** IFN bioassays of macrophages transfected with the indicated 2-5A species at 5 mM and harvested 8 hours later.

**(d)** Bioanalyzer profiles of cellular RNA harvested from WT (top row) and *Rnasel-/-* (bottom row) macrophages. The positions of 18S and 28S rRNA are indicated.

**(e)** IFN bioassays of macrophages transfected with the indicated ligands and harvested 8 hours later.

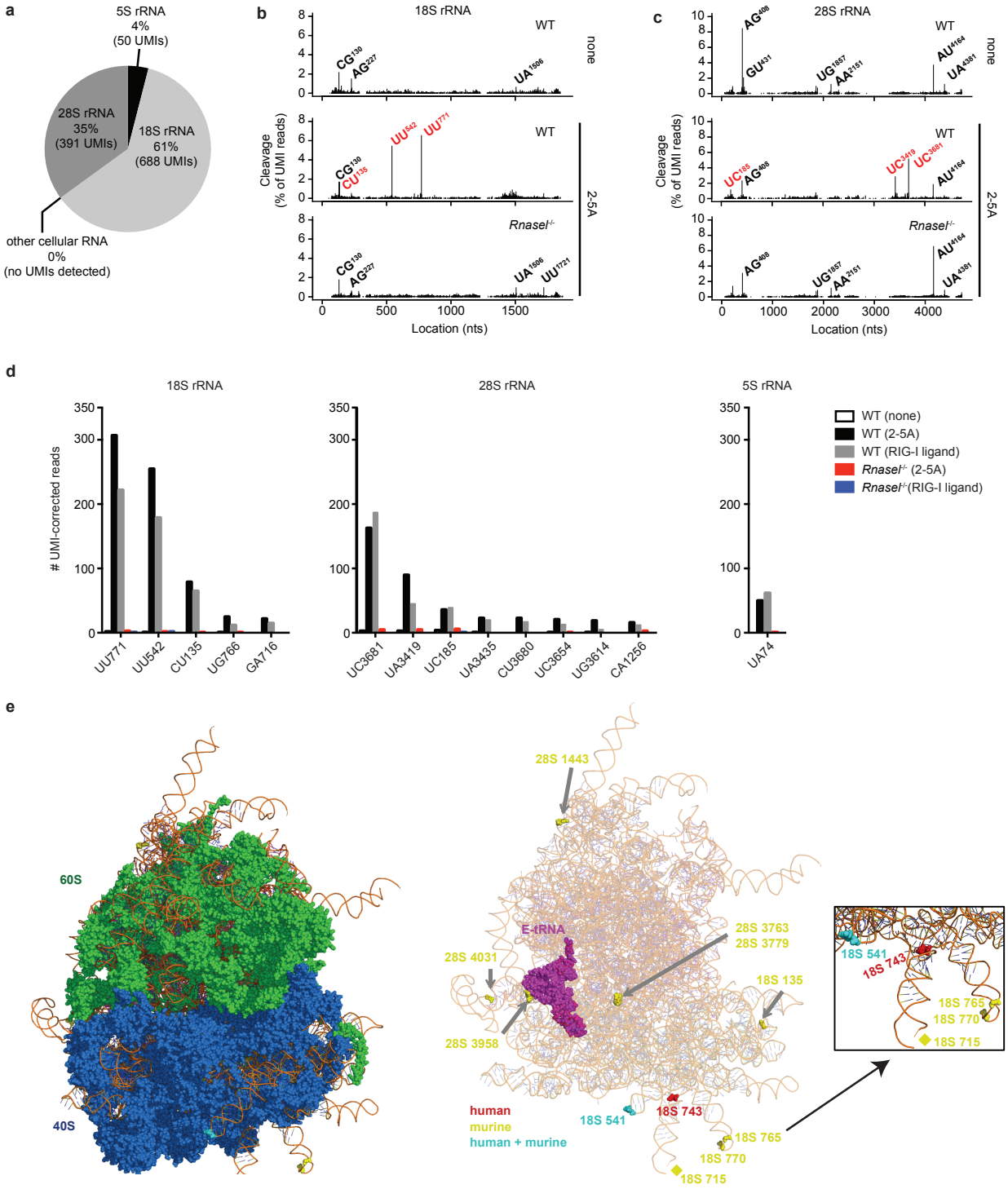


*Figure 3.4: RNase L uniquely targets rRNA in vivo*

**(a)** RNase L-dependent RNA cleavage sites were defined as sites with >10-fold induction of UMI-corrected reads in treated WT cells compared to untreated WT cells, with no induction in *Rnasel*-/- cells. The graph depicts the mapped locations of all RNase L-dependent sites.

**(b-c)** Mapping of UMI-corrected 3' phosphate RNAs to 18s rRNA (**b**) and 28s rRNA (**c**). RNase L-dependent signals are highlighted in red.

(**d**) All RNase L-dependent rRNA cleavage sites, expressed as UMI-corrected reads, are depicted for 18s, 28s, and 5s rRNA.

(**e**) RNase L-dependent rRNA cleavage sites were mapped to the human ribosome. The left image includes ribosomal proteins, the center image depicts just rRNA, and the right image highlights a densely targeted region of 18s rRNA. Sites from in murine cells are yellow, sites from human cells are in red, and a shared site in murine and human cells is in cyan. The position of the tRNA on the translating ribosome is shown in magenta.

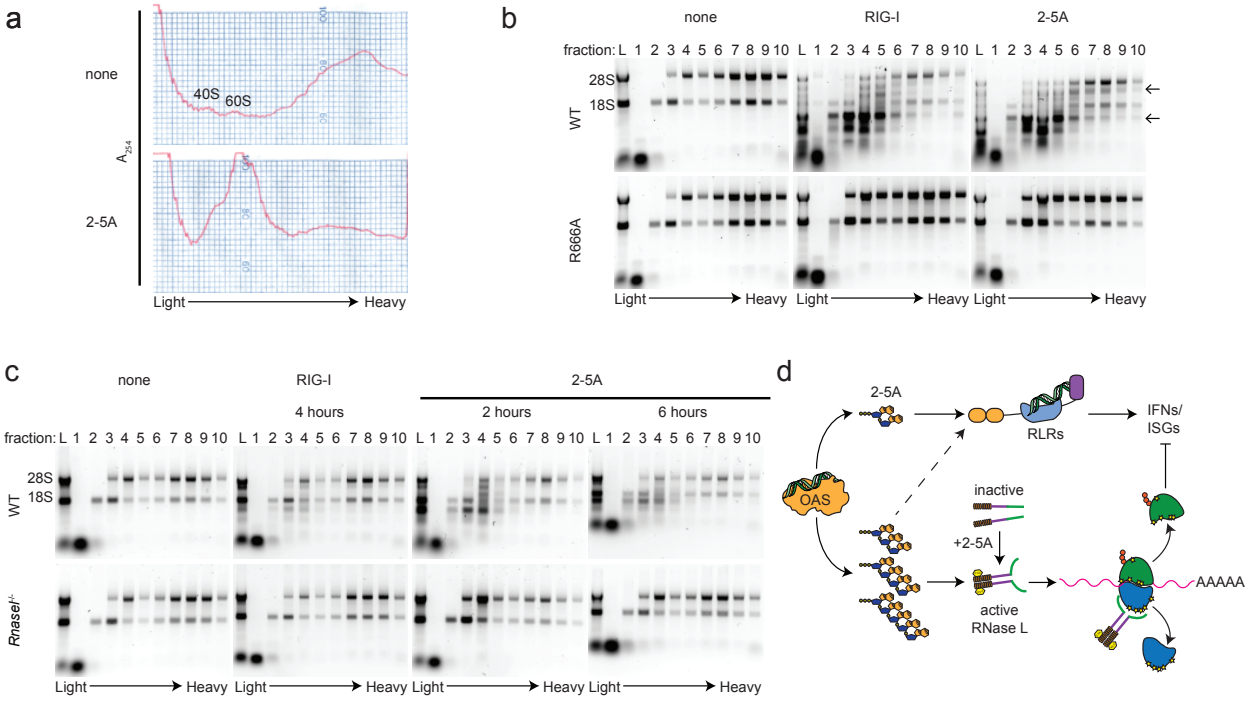


*Figure 4.4: RNase L inactivates ribosomes*

**(a)** Immortalized MEFs expressing epitope-tagged RNase L were treated with 2-5A and harvested two hours post treatment. Polysome extracts were fractionated, and the OD254 absorption profiles are shown.

**(b)** RNA gels depicting rRNA distribution and integrity across the gradients are shown for cells expressing WT RNase L (top row) and R666A RNase L (bottom row). Arrows indicate the positions of major cleavage products of rRNA that can be found throughout the gradient of cells expression WT RNase L, but not catalytic mutant RNase L.

**(c)** Primary bone marrow macrophages WT mice (top row) and Rnasel-/- mice (bottom row) were treated and analyzed for rRNA distribution as in (**b**).

**(d)** Revised model of the function of OAS, 2-5A, and RNase L. 2-5A molecules are both RNase L activators and endogenous RLR ligands, and RNase L functions to inactivate ribosomes, limiting the antiviral response.

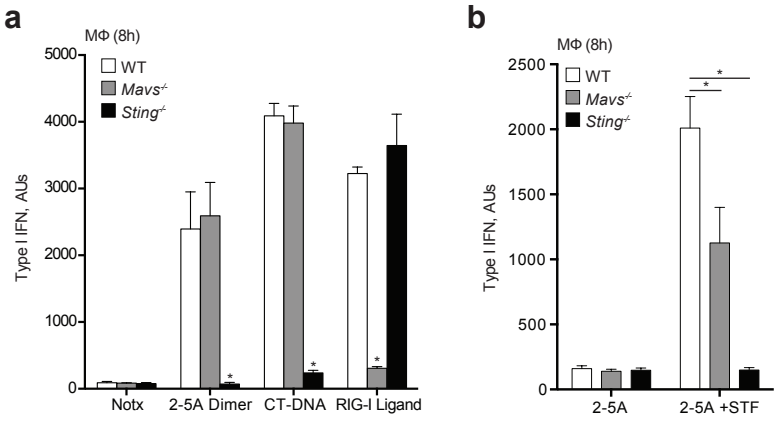


*Figure 4.5: 2-5A interferon induction is STING dependent*

**(a)** IFN bioassays of primary bone marrow derived macrophages transfected with the indicated ligands and harvested 8 hours later.

**(b)** The same cells as above were transfected with 2-5A in the presence or absence of STF.

# Chapter 3 Extended Data

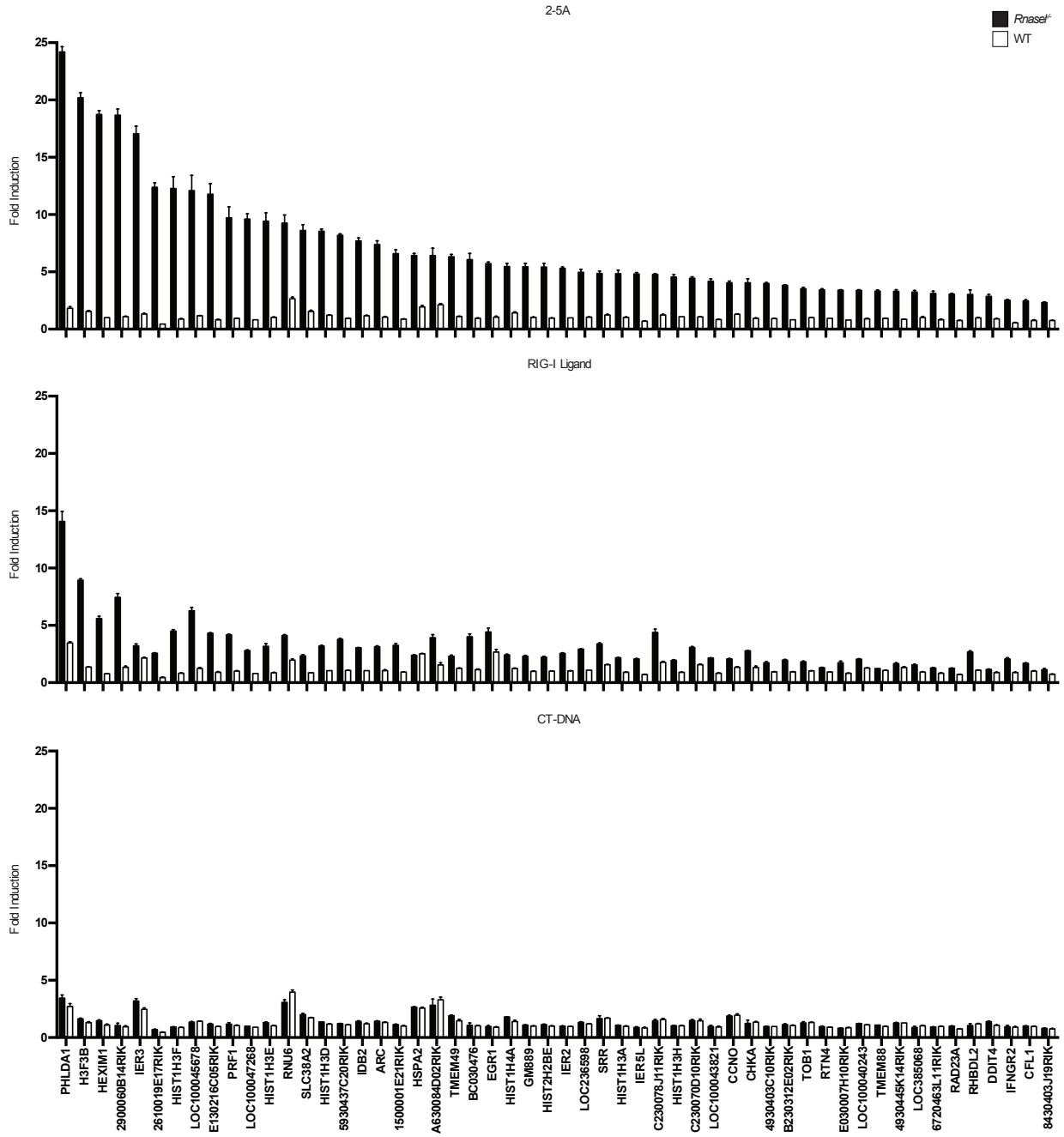


*Extended Data Figure 3.1: RNase L-Dependent Genes*

Shown are the 54 most highly induced genes dependent on RNase L expression and activation. All samples were harvested after a 4 hour stimulation.

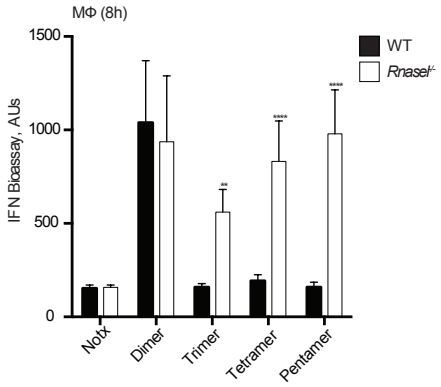


*Extended Data Figure 3.2: 2-5A Species Induce Type I Interferon*

IFN bioassays of macrophages transfected with the indicated 2-5A species at 5 mM and harvested 8 hours later.

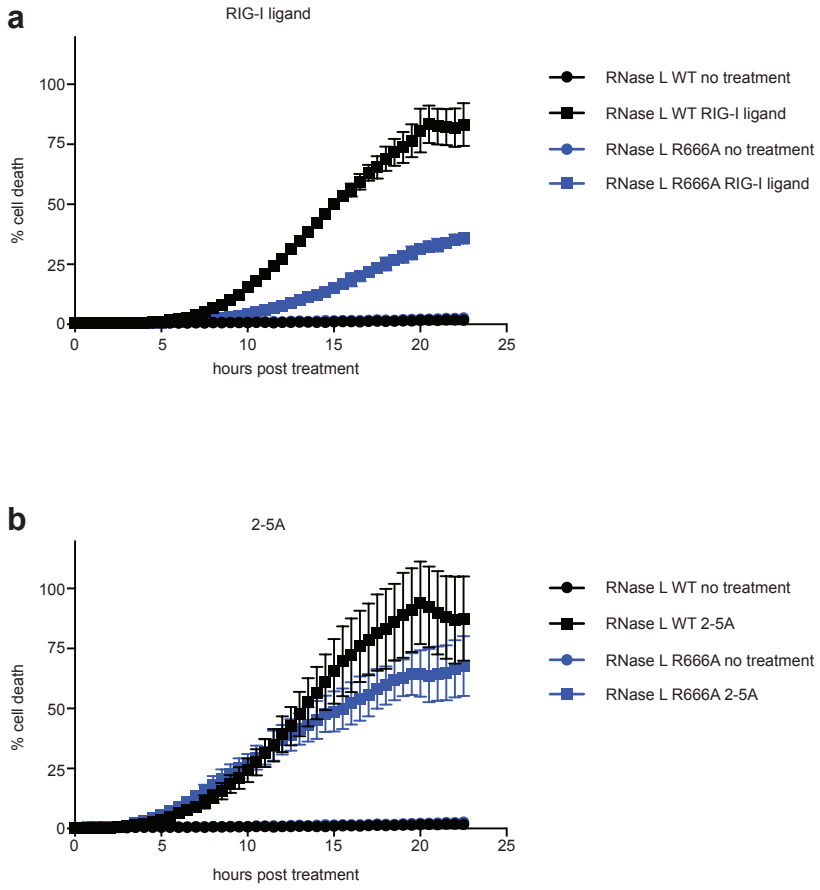


*Extended Data Figure 3.3: Catalytic activity of RNase L does not lead to rapid cell death*

**(a)** Immortalized murine fibroblasts expressing WT RNase L or the R666A catalytic mutant were treated with RIG-I and analyzed using quantitative live cell imaging for the time course listed on an IncuCyte device.

**(b)** Cells were treated with 2-5A and analyzed as above.

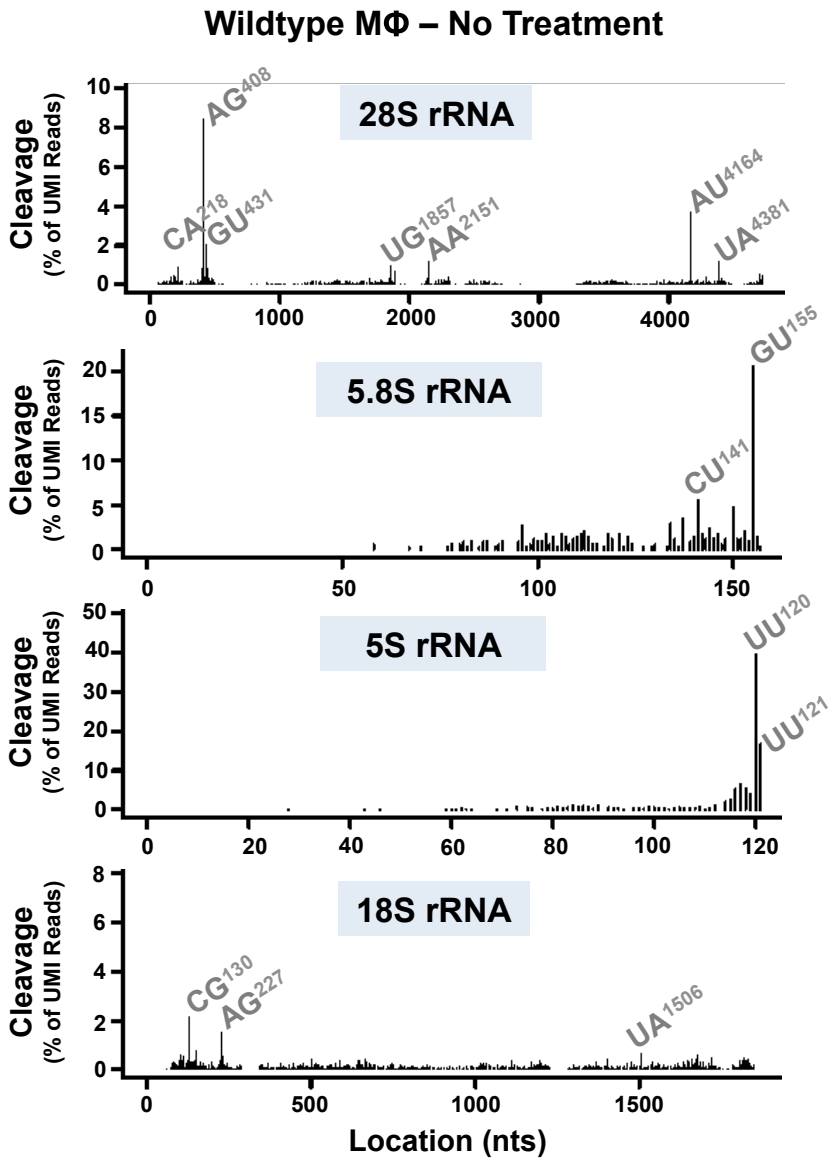


*Extended Data Figure 3.4: Frequency and location of cleavage sites in rRNAs*

Data from Extended Data Tables 3-9.

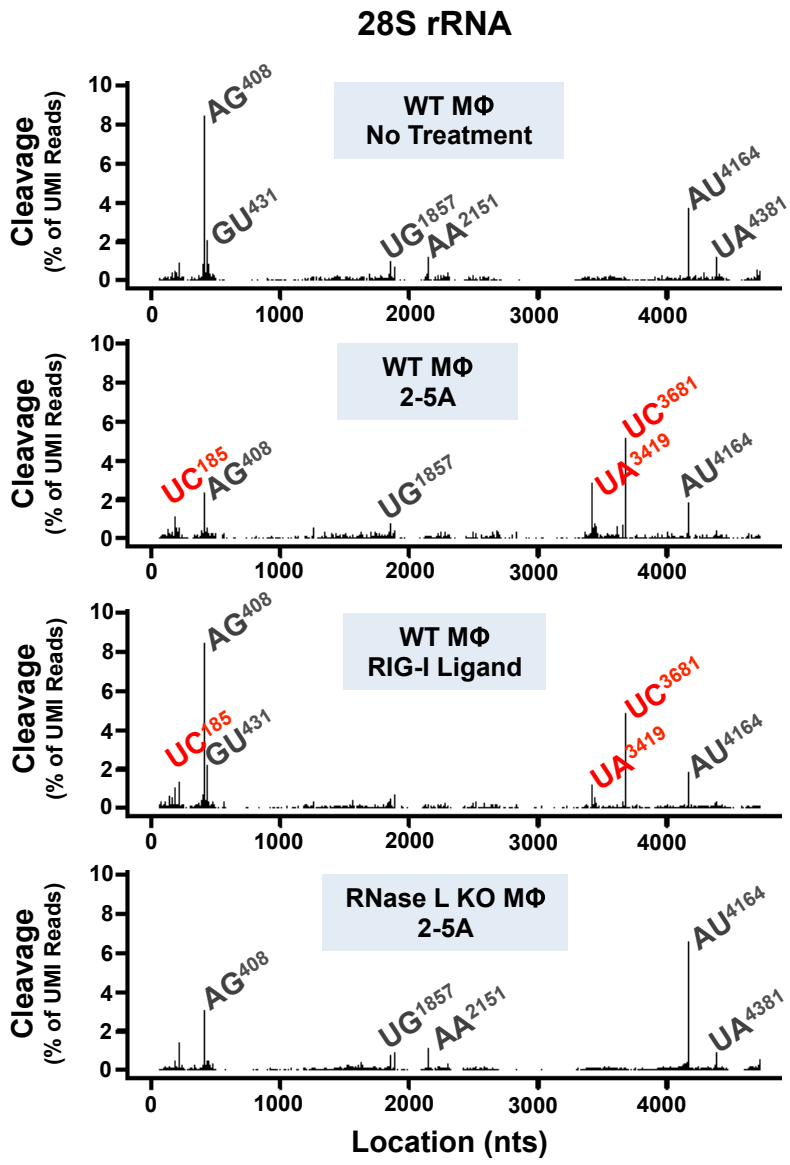


*Extended Data Figure 3.5: Frequency and location of cleavage sites in 28s rRNAs*

Data from Extended Data Tables 3 & 4. Prominent RNase L-dependent cleavage sites annotated in red.

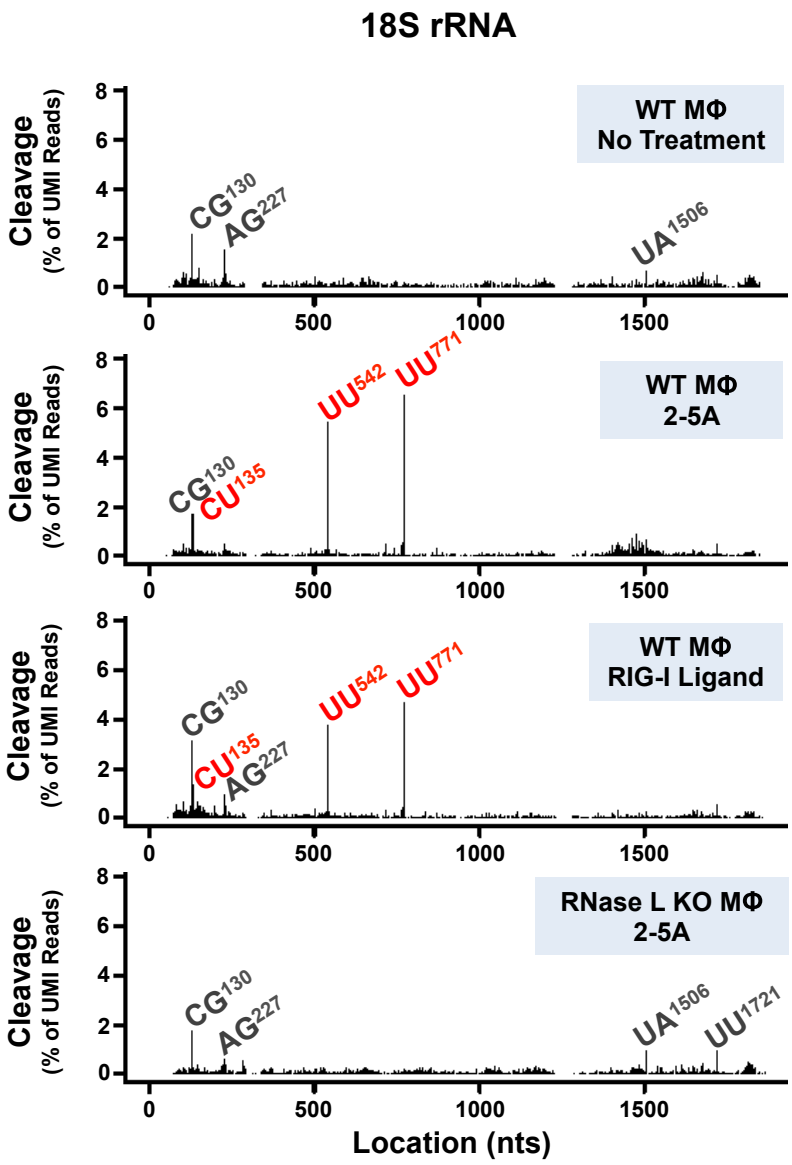


*Extended Data Figure 3.6: Frequency and location of cleavage sites in 18s rRNAs*

Data from Extended Data Tables 5 & 6. Prominent RNase L-dependent cleavage sites annotated in red.

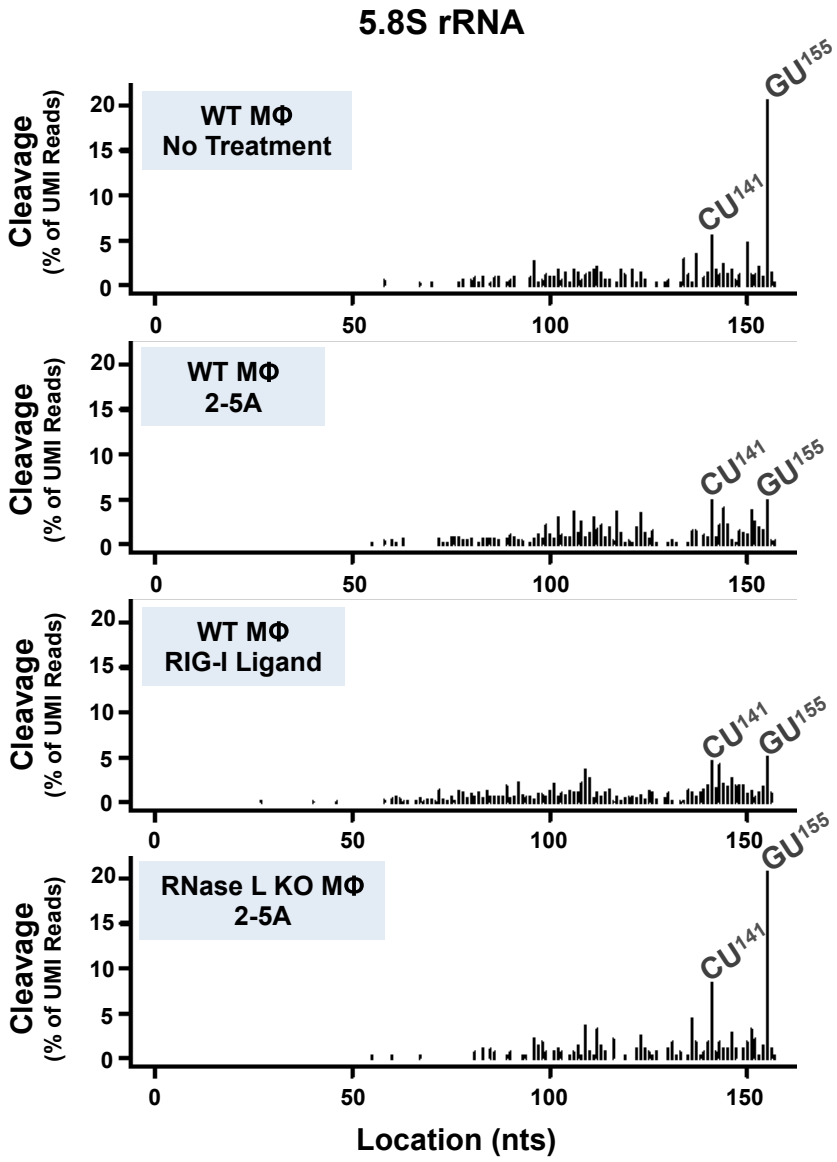


*Extended Data Figure 3.7: Frequency and location of cleavage sites in 5.8s rRNAs*

Data derived from Extended Data Table 7.

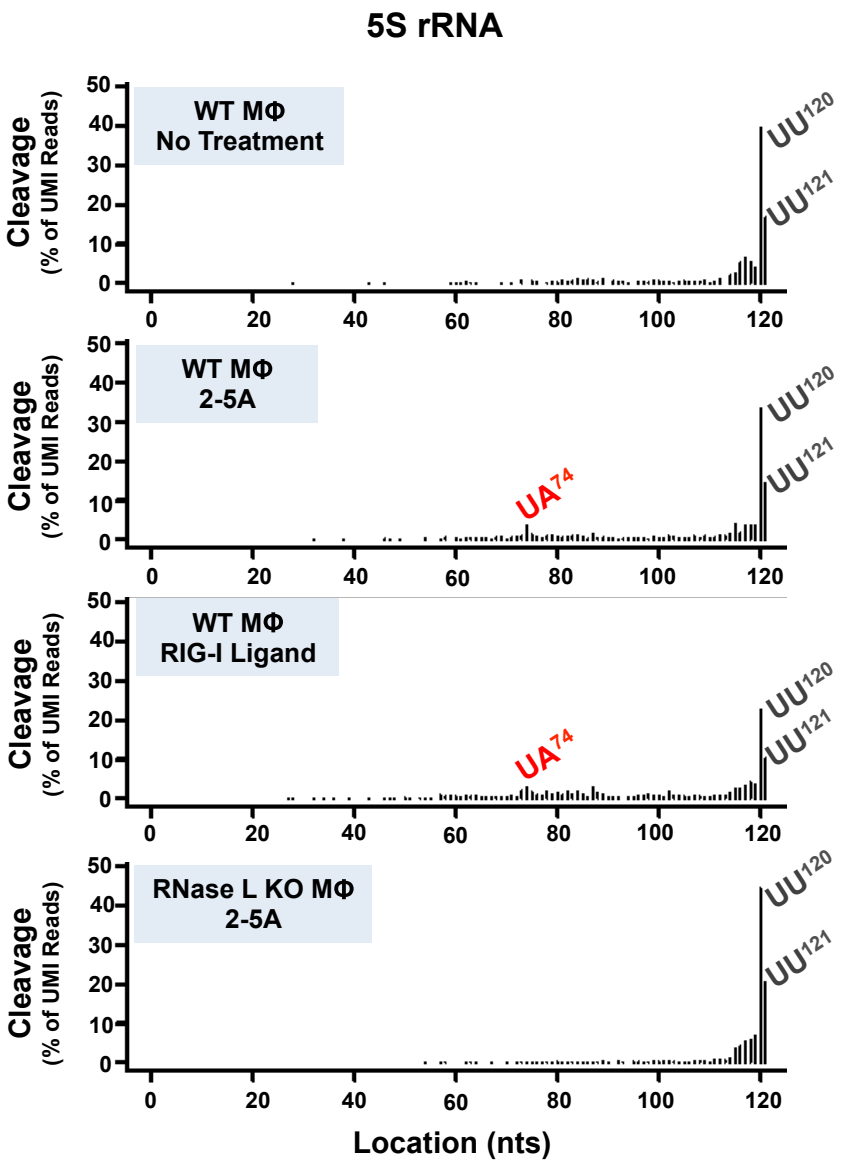


*Extended Data Figure 3.8: Frequency and location of cleavage sites in 5s rRNAs*

Data from Extended Data Tables 8 & 9. RNase L-dependent cleavage sites annotated in red.

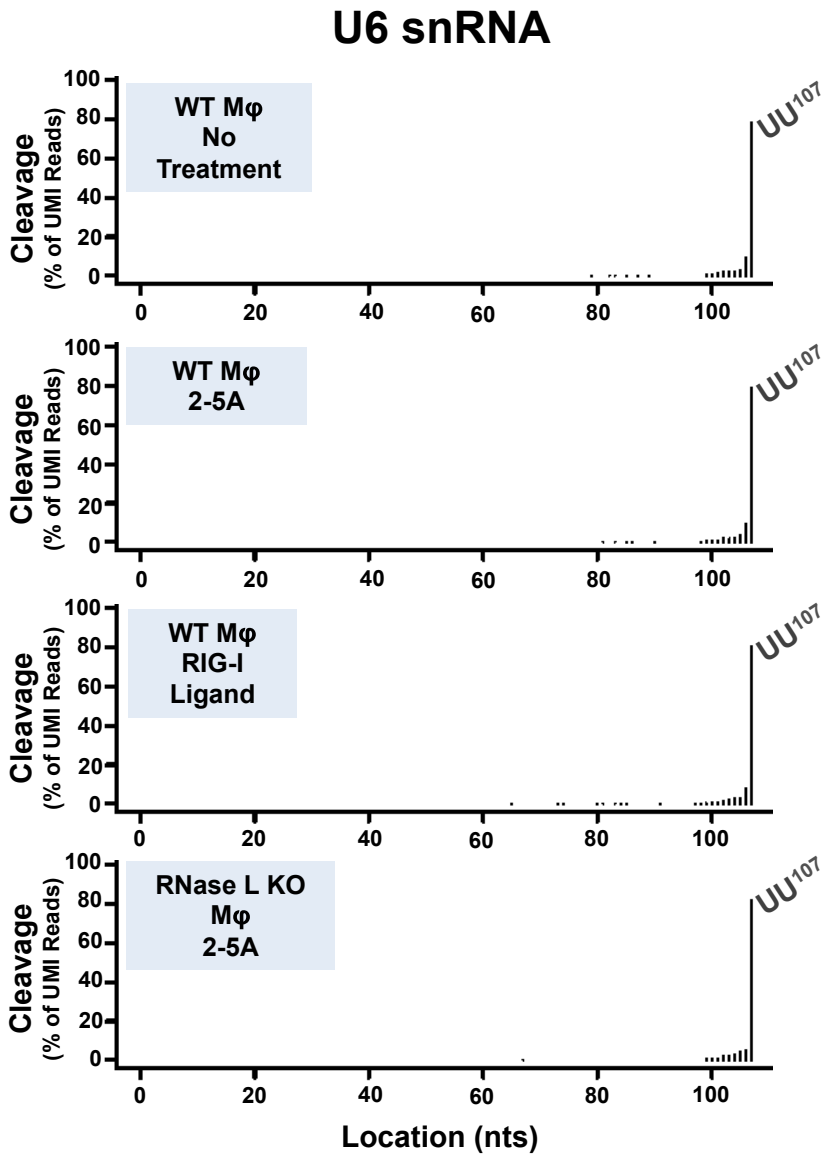


*Extended Data Figure 3.9: Frequency and location of cleavage sites in U6 snRNA*

Data from Extended Data Tables 10 & 11.

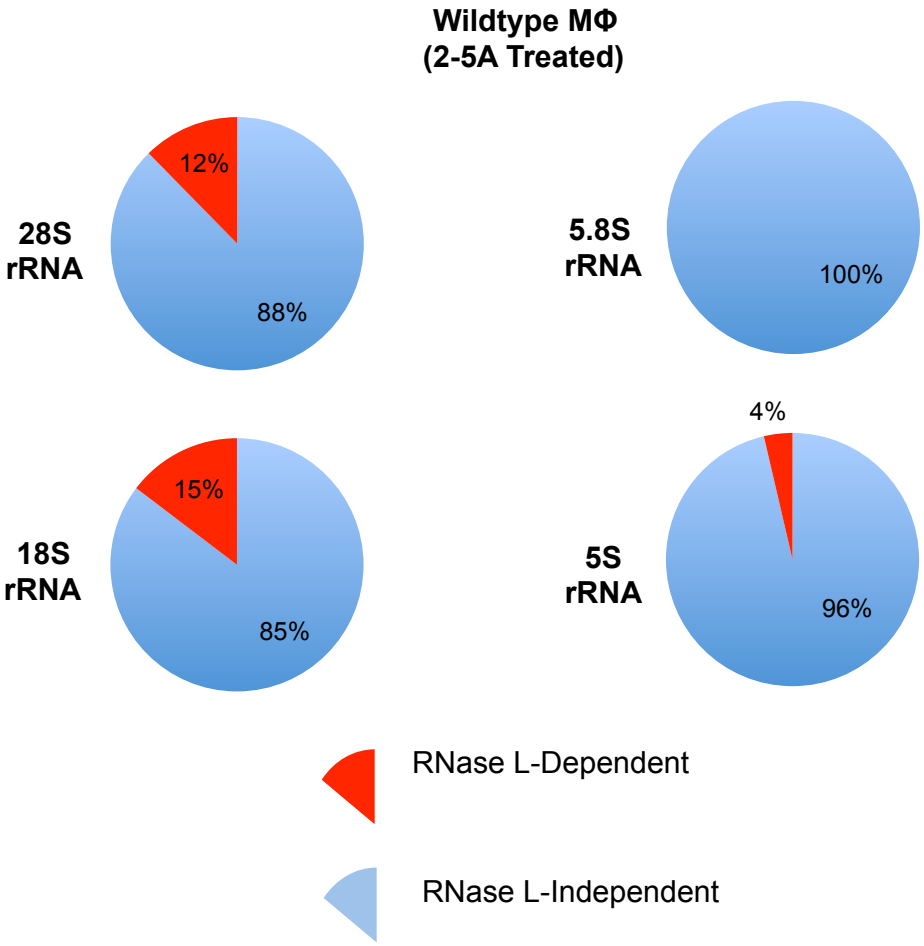


*Extended Data Figure 3.10: RNase L-dependent and -independent cleavage sites in ribosomal RNAs*

Percent of UMI-corrected cleavage in each RNA. Data from Extended Data Tables 2-9.

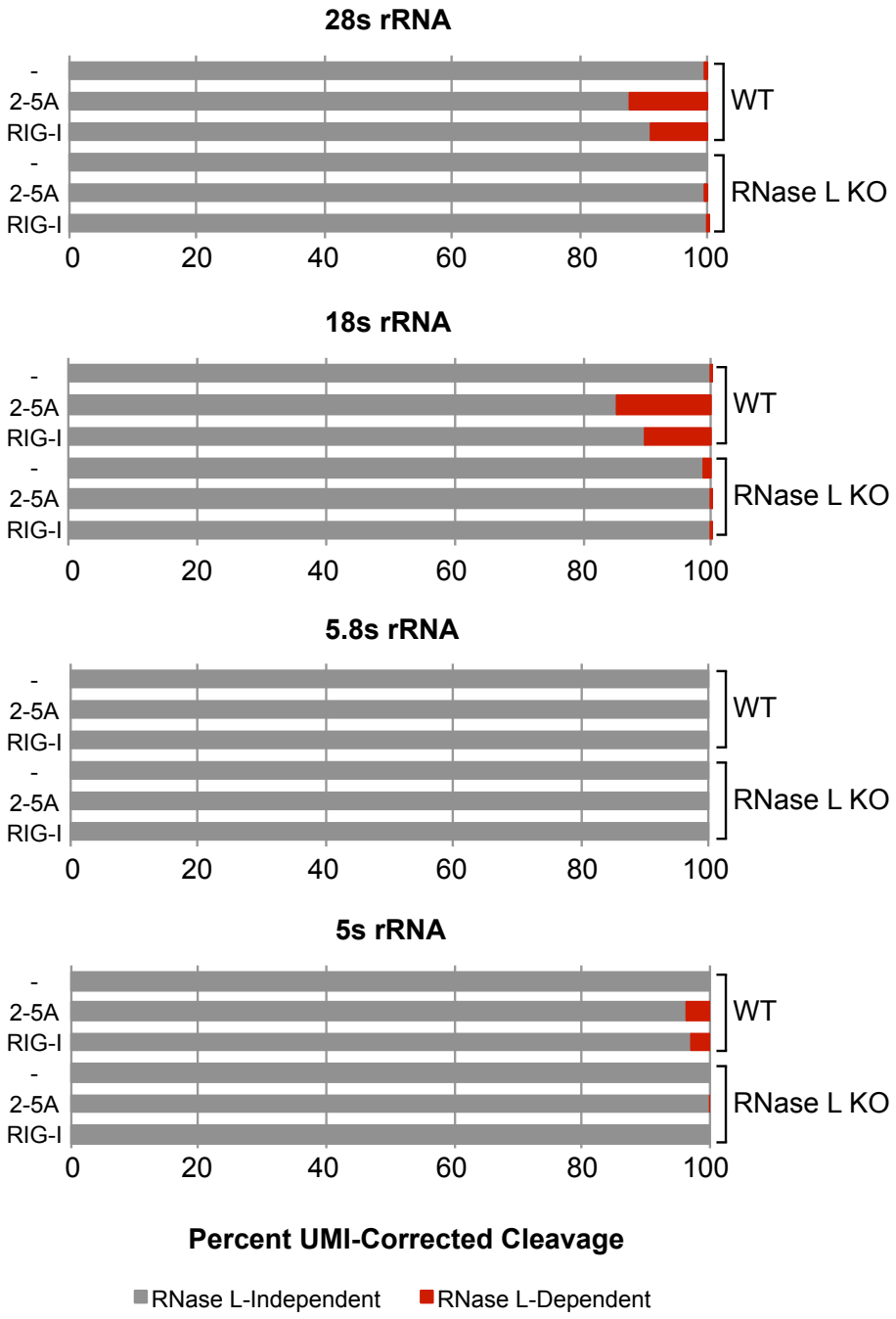


*Extended Data Figure 3.11: RNase L-dependent and -independent cleavage sites in ribosomal RNAs*

RNase L-dependent (red) and RNase L-independent (grey) cleavage frequency.

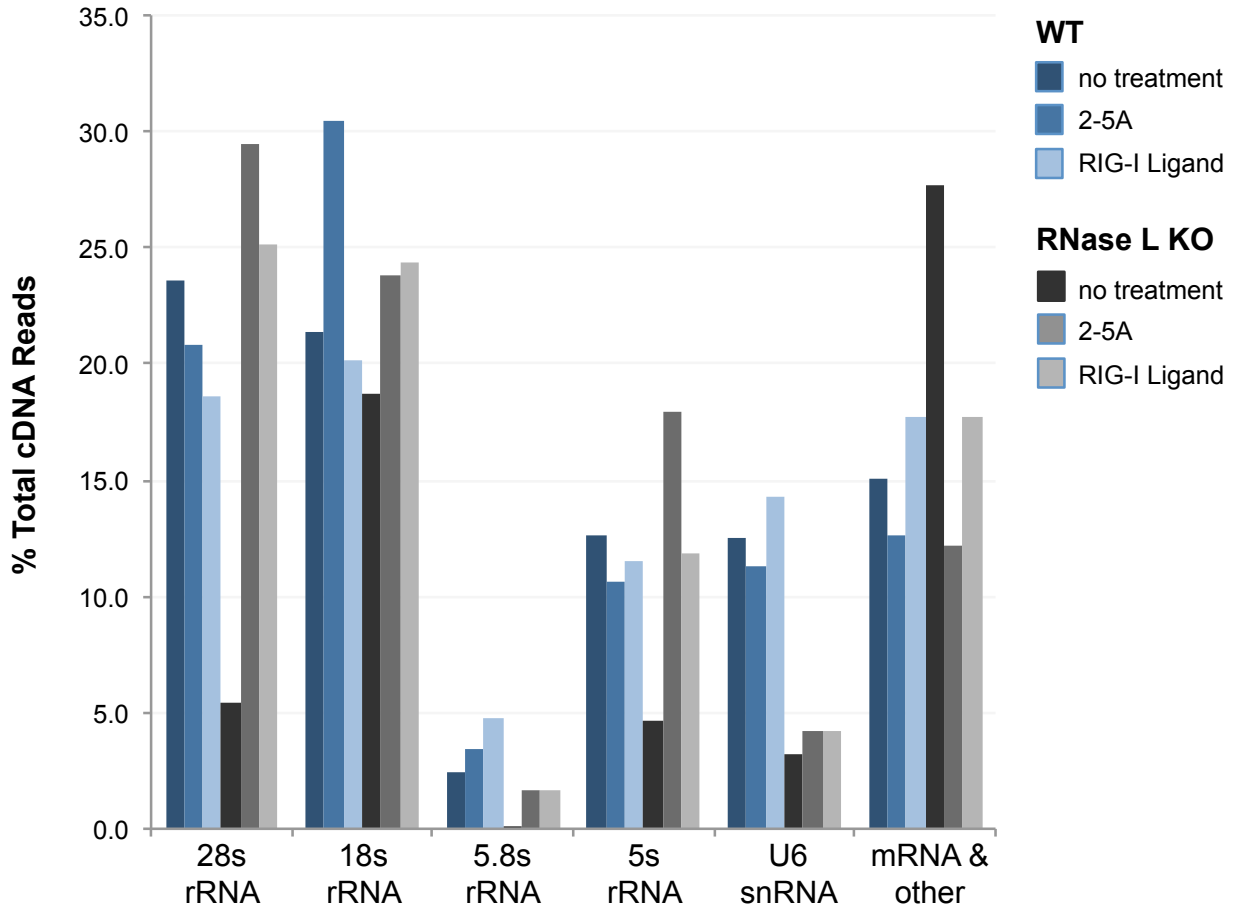


*Extended Data Figure 3.12: Percent of total cDNA reads aligned to cellular RNAs*

Data from Extended Data Table 1

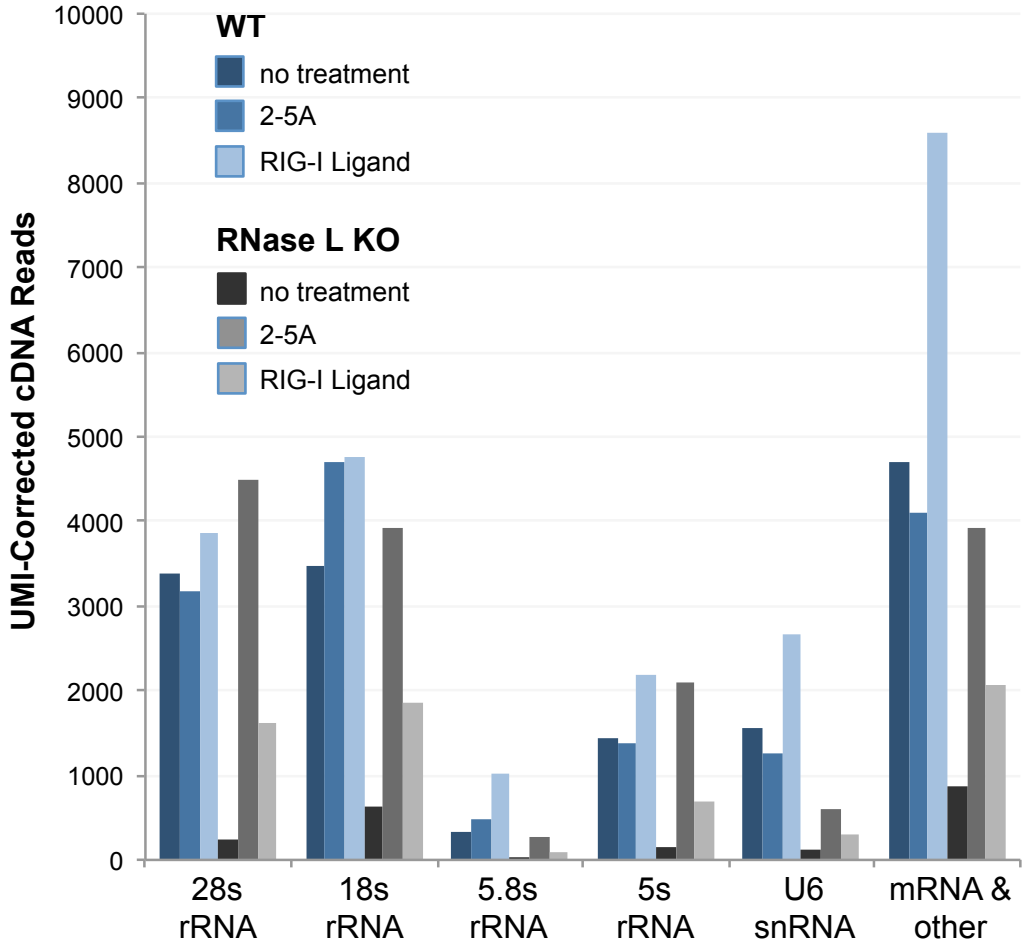


*Extended Data Figure 3.13: Cellular RNAs with cyclic phosphates*

Data from Extended Data Table 2.

| | Wildtype Macrophage (treatment) | | | RNase L -/- Macrophage (treatment) | | |
|---|---|---|---|---|---|---|
| | (None) | (2-5A) | (RIG-I Ligand) | (None) | (2-5A) | (RIG-I Ligand) |
| cDNA Reads (%) | 955,372 (100) | 873,035 (100) | 992,456 (100) | 690,412 (100) | 726,586 (100) | 899,914 (100) |
| 28S rRNA (%) | 224,932 (23.5) | 181,861 (20.8) | 184,254 (18.6) | 37,630 (5.5) | 213,686 (29.4) | 226,394 (25.2) |
| 18S rRNA (%) | 204,431 (21.4) | 265,992 (30.5) | 200,428 (20.2) | 129,059 (18.7) | 172,746 (23.8) | 219,333 (24.4) |
| 5.8S rRNA (%) | 23,775 (2.5) | 30,117 (3.4) | 46,899 (4.7) | 491 (0.1) | 11,735 (1.6) | 14,623 (1.6) |
| 5S rRNA (%) | 121,046 (12.7) | 92,423 (10.6) | 114,470 (11.5) | 32,405 (4.7) | 130,285 (17.9) | 106,635 (11.8) |
| U6 snRNA (%) | 119,803 (12.5) | 98,214 (11.2) | 142,200 (14.3) | 21,819 (3.2) | 30,171 (4.2) | 37,397 (4.2) |
| mRNA & other (%) | 143,724 (15.0) | 110,522 (12.7) | 175,626 (17.7) | 191,515 (27.7) | 88,488 (12.2) | 159,013 (17.7) |
| Unaligned (%) | 117,661 (12.3) | 93,906 (10.8) | 128,579 (13.0) | 277,493 (40.2) | 79,475 (10.9) | 136,519 (15.2) |

*Extended Data Tables 1: Total cDNA reads and percent aligned to particular RNAs*

Raw sequences were trimmed of residual linker sequences and aligned in the following order using Bowtie with options -m 1 --best --strata --un to *Mus musculus* 28S rRNA (NR_003279.1), 18S rRNA (NR_003278.3), 5.8S rRNA (NR_003280.2), 5S rRNA (NR_046153.1), U6 snRNA (NR_003027.2). Remaining sequences were aligned to NCBI37/mm9 using Bowtie with the -m 100 --best --strata –un options.
from Extended Data Table 2.

| | Wildtype Macrophage | | | RNase L -/- Macrophage | | |
|---|---|---|---|---|---|---|
| Treatment: | None | 2-5A | RIG-I Ligand | None | 2-5A | RIG-I Ligand |
| 28S rRNA | 3379 | 3169 | 3864 | 235 | 4501 | 1630 |
| 18S rRNA | 3482 | 4696 | 4761 | 637 | 3926 | 1851 |
| 5.8S rRNA | 340 | 470 | 1025 | 21 | 276 | 106 |
| 5S rRNA | 1426 | 1375 | 2198 | 148 | 2096 | 685 |
| U6 snRNA | 1560 | 1250 | 2651 | 110 | 611 | 303 |
| mRNA & Other | 4698 | 4100 | 8606 | 862 | 3935 | 2055 |

*Extended Data Tables 2: UMI-corrected cDNA reads in dataset*

| | Wildtype Macrophage (treatment) | | | RNase L -/- Macrophage (treatment) | | |
|---|---|---|---|---|---|---|
| Position | (None) | (2-5A) | (RIG-I Ligand) | (None) | (2-5A) | (RIG-I Ligand) |
| UC$^{3681}$ | 3 | 163 | 187 | 0 | 5 | 0 |
| UA$^{3419}$ | 3 | 90 | 45 | 0 | 5 | 0 |
| AG$^{408}$ | 285 | 73 | 326 | 10 | 138 | 69 |
| AU$^{4164}$ | 125 | 58 | 71 | 5 | 295 | 103 |
| UC$^{185}$ | 4 | 36 | 39 | 0 | 6 | 1 |
| UG$^{1857}$ | 32 | 24 | 17 | 1 | 33 | 16 |
| UA$^{3435}$ | 1 | 23 | 20 | 0 | 0 | 0 |
| CU$^{3680}$ | 0 | 23 | 17 | 0 | 0 | 0 |
| UC$^{3654}$ | 1 | 21 | 13 | 0 | 1 | 0 |
| UA$^{3455}$ | 2 | 20 | 10 | 1 | 2 | 1 |
| UG$^{3614}$ | 1 | 19 | 5 | 0 | 0 | 0 |
| UU$^{3429}$ | 3 | 18 | 6 | 0 | 3 | 8 |
| AA$^{198}$ | 4 | 17 | 2 | 0 | 0 | 0 |
| CA$^{218}$ | 31 | 17 | 52 | 1 | 62 | 10 |
| CA$^{1256}$ | 0 | 16 | 12 | 0 | 3 | 0 |
| GU$^{431}$ | 69 | 16 | 84 | 3 | 20 | 27 |
| CG$^{134}$ | 1 | 15 | 2 | 0 | 3 | 3 |
| CA$^{197}$ | 2 | 14 | 6 | 0 | 1 | 1 |
| UG$^{188}$ | 15 | 13 | 9 | 1 | 12 | 8 |
| GC$^{1885}$ | 24 | 13 | 2 | 1 | 39 | 14 |

*Extended Data Tables 3: UMI-corrected cDNA reads in 28s rRNA*

* 20 most frequent cleavage sites (benchmarked to wild type macrophages treated with 2-5A).

Number of UMI reads corresponding to a cyclic phosphate at each position in 28S rRNA.

Red: 2-5A activated cleavage sites / RIG-I ligand activated cleavage sites / RNase L-dependent ≥ 10-fold activation in wild type macrophages and little-to-no activation in RNASE L -/- macrophages

| | Wildtype Macrophage (treatment) | | | RNase L -/- Macrophage (treatment) | | |
|---|---|---|---|---|---|---|
| Position | (None) | (2-5A) | (RIG-I Ligand) | (None) | (2-5A) | (RIG-I Ligand) |
| UC$^{3681}$ | 0.1 | 5.1 | 4.8 | 0.0 | 0.1 | 0.0 |
| UA$^{3419}$ | 0.1 | 2.8 | 1.2 | 0.0 | 0.1 | 0.0 |
| AG$^{408}$ | 8.4 | 2.3 | 8.4 | 4.3 | 3.1 | 4.2 |
| AU$^{4164}$ | 3.7 | 1.8 | 1.8 | 2.1 | 6.6 | 6.3 |
| UC$^{185}$ | 0.1 | 1.1 | 1.0 | 0.0 | 0.1 | 0.1 |
| UG$^{1857}$ | 0.9 | 0.8 | 0.4 | 0.4 | 0.7 | 1.0 |
| UA$^{3435}$ | 0.0 | 0.7 | 0.5 | 0.0 | 0.0 | 0.0 |
| CU$^{3680}$ | 0.0 | 0.7 | 0.4 | 0.0 | 0.0 | 0.0 |
| UC$^{3654}$ | 0.0 | 0.7 | 0.3 | 0.0 | 0.0 | 0.0 |
| UA$^{3455}$ | 0.1 | 0.6 | 0.3 | 0.4 | 0.0 | 0.1 |
| UG$^{3614}$ | 0.0 | 0.6 | 0.1 | 0.0 | 0.0 | 0.0 |
| UU$^{3429}$ | 0.1 | 0.6 | 0.2 | 0.0 | 0.1 | 0.5 |
| AA$^{198}$ | 0.1 | 0.5 | 0.1 | 0.0 | 0.0 | 0.0 |
| CA$^{218}$ | 0.9 | 0.5 | 1.3 | 0.4 | 1.4 | 0.6 |
| CA$^{1256}$ | 0 | 0.5 | 0.3 | 0.0 | 0.1 | 0.0 |
| GU$^{431}$ | 2.0 | 0.5 | 2.2 | 1.3 | 0.4 | 1.7 |
| CG$^{134}$ | 0.0 | 0.5 | 0.1 | 0.0 | 0.1 | 0.2 |
| CA$^{197}$ | 0.1 | 0.4 | 0.2 | 0.0 | 0.0 | 0.1 |
| UG$^{188}$ | 0.4 | 0.4 | 0.2 | 0.4 | 0.3 | 0.5 |
| GC$^{1885}$ | 0.7 | 0.4 | 0.7 | 0.4 | 0.9 | 0.9 |

*Extended Data Tables 4: Percentage of cleavage at individual sites in 28s rRNA*

* 20 most frequent cleavage sites (benchmarked to wild type macrophages treated with 2-5A).

Percentage of cleavage at individual sites in 28s rRNA (% of UMI-corrected reads in 28s rRNA).

Red: 2-5A activated cleavage sites / RIG-I ligand activated cleavage sites / RNase L-dependent ≥ 10-fold activation in wild type macrophages and little-to-no activation in RNASE L -/- macrophages

| | Wildtype Macrophage (treatment) | | | RNase L -/- Macrophage (treatment) | | |
|---|---|---|---|---|---|---|
| Position | (None) | (2-5A) | (RIG-I Ligand) | (None) | (2-5A) | (RIG-I Ligand) |
| UU$^{771}$ | 2 | 307 | 222 | 1 | 3 | 1 |
| UU$^{542}$ | 1 | 255 | 179 | 4 | 2 | 2 |
| CG$^{130}$ | 75 | 79 | 150 | 6 | 69 | 31 |
| CU$^{135}$ | 0 | 79 | 65 | 1 | 1 | 0 |
| AU$^{1477}$ | 10 | 41 | 5 | 0 | 8 | 8 |
| UU$^{1463}$ | 5 | 33 | 3 | 1 | 9 | 0 |
| UA$^{1506}$ | 22 | 32 | 12 | 1 | 37 | 10 |
| UA$^{1486}$ | 0 | 27 | 4 | 0 | 4 | 0 |
| CG$^{1420}$ | 1 | 26 | 16 | 0 | 5 | 0 |
| UC$^{1493}$ | 3 | 25 | 7 | 0 | 2 | 0 |
| UG$^{766}$ | 1 | 25 | 12 | 2 | 1 | 0 |
| AG$^{227}$ | 52 | 24 | 46 | 1 | 24 | 11 |
| UA$^{102}$ | 20 | 23 | 30 | 0 | 10 | 0 |
| UU$^{1721}$ | 16 | 23 | 25 | 5 | 37 | 11 |
| GC$^{131}$ | 8 | 22 | 44 | 1 | 10 | 8 |
| CA$^{1454}$ | 2 | 22 | 0 | 0 | 1 | 0 |
| CA$^{1483}$ | 7 | 22 | 8 | 0 | 3 | 1 |
| GA$^{716}$ | 0 | 22 | 15 | 0 | 0 | 0 |
| UC$^{129}$ | 5 | 21 | 21 | 1 | 7 | 1 |
| AC$^{1403}$ | 15 | 21 | 4 | 0 | 3 | 3 |

*Extended Data Tables 5: UMI-corrected cDNA reads in 18s rRNA*

* 20 most frequent cleavage sites (benchmarked to wild type macrophages treated with 2-5A).

Number of UMI reads corresponding to a cyclic phosphate at each position in 18S rRNA.

Red: 2-5A activated cleavage sites / RIG-I ligand activated cleavage sites / RNase L-dependent ≥ 10-fold activation in wild type macrophages and little-to-no activation in RNASE L -/- macrophages

| | Wildtype Macrophage (treatment) | | | RNase L -/- Macrophage (treatment) | | |
|---|---|---|---|---|---|---|
| Position | (None) | (2-5A) | (RIG-I Ligand) | (None) | (2-5A) | (RIG-I Ligand) |
| UU$^{771}$ | 0.1 | 6.5 | 4.7 | 0.2 | 0.1 | 0.1 |
| UU$^{542}$ | 0.0 | 5.4 | 3.8 | 0.6 | 0.1 | 0.1 |
| CG$^{130}$ | 2.2 | 1.7 | 3.2 | 0.9 | 1.8 | 1.7 |
| CU$^{135}$ | 0.0 | 1.7 | 1.4 | 0.2 | 0.0 | 0.0 |
| AU$^{1477}$ | 0.3 | 0.9 | 0.1 | 0.0 | 0.2 | 0.4 |
| UU$^{1463}$ | 0.1 | 0.7 | 0.1 | 0.2 | 0.2 | 0.0 |
| UA$^{1506}$ | 0.6 | 0.7 | 0.3 | 0.0 | 0.9 | 0.5 |
| UA$^{1486}$ | 0.0 | 0.6 | 0.1 | 0.3 | 0.1 | 0.0 |
| CG$^{1420}$ | 0.0 | 0.6 | 0.3 | 0.0 | 0.1 | 0.0 |
| UC$^{1493}$ | 0.1 | 0.5 | 0.1 | 0.0 | 0.1 | 0.0 |
| UG$^{766}$ | 0.0 | 0.5 | 0.3 | 0.3 | 0.0 | 0.0 |
| AG$^{227}$ | 1.5 | 0.5 | 1.0 | 0.2 | 0.6 | 0.6 |
| UA$^{102}$ | 0.6 | 0.5 | 0.6 | 0.0 | 0.3 | 0.0 |
| UU$^{1721}$ | 0.5 | 0.5 | 0.5 | 0.8 | 0.9 | 0.6 |
| GC$^{131}$ | 0.2 | 0.5 | 0.9 | 0.2 | 0.3 | 0.4 |
| CA$^{1454}$ | 0.1 | 0.5 | 0.0 | 0.0 | 0.0 | 0.0 |
| CA$^{1483}$ | 0.2 | 0.5 | 0.2 | 0.0 | 0.1 | 0.1 |
| GA$^{716}$ | 0.0 | 0.5 | 0.3 | 0.0 | 0.0 | 0.0 |
| UC$^{129}$ | 0.1 | 0.4 | 0.4 | 0.2 | 0.2 | 0.1 |
| AC$^{1403}$ | 0.4 | 0.4 | 0.1 | 0.0 | 0.1 | 0.2 |

*Extended Data Tables 6: Percentage of cleavage at individual sites in 18s rRNA*

* 20 most frequent cleavage sites (benchmarked to wild type macrophages treated with 2-5A).

Percentage of cleavage at individual sites in 18s rRNA (% of UMI-corrected reads in 18s rRNA).

Red: 2-5A activated cleavage sites / RIG-I ligand activated cleavage sites / RNase L-dependent $\geq$ 10-fold activation in wild type macrophages and little-to-no activation in RNASE L -/- macrophages

| | Wildtype Macrophage (treatment) | | | RNase L -/- Macrophage (treatment) | | |
|---|---|---|---|---|---|---|
| Position | (None) | (2-5A) | (RIG-I Ligand) | (None) | (2-5A) | (RIG-I Ligand) |
| $GU^{155}$ | 70 | 23 | 52 | 2 | 57 | 22 |
| $CU^{141}$ | 19 | 23 | 47 | 1 | 23 | 8 |
| $UC^{144}$ | 8 | 19 | 21 | 0 | 3 | 5 |
| $GU^{151}$ | 4 | 18 | 13 | 1 | 9 | 3 |
| $GC^{106}$ | 6 | 17 | 11 | 0 | 2 | 0 |
| $CC^{117}$ | 1 | 17 | 7 | 0 | 0 | 0 |
| $UU^{123}$ | 5 | 16 | 8 | 0 | 7 | 3 |
| $GA^{102}$ | 6 | 14 | 7 | 0 | 3 | 0 |
| $UG^{111}$ | 6 | 14 | 5 | 0 | 1 | 0 |
| $AC^{108}$ | 2 | 12 | 22 | 1 | 1 | 0 |

*Extended Data Tables 7: UMI-corrected cDNA reads in 5.8s rRNA*

* 20 most frequent cleavage sites (benchmarked to wild type macrophages treated with 2-5A).

Number of UMI reads corresponding to a cyclic phosphate at each position in 5.8S rRNA.

$CC^{117}$ weakly consistent with RNase L-dependent criteria.

| | Wildtype Macrophage (treatment) | | | RNase L -/- Macrophage (treatment) | | |
|---|---|---|---|---|---|---|
| Position | (None) | (2-5A) | (RIG-I Ligand) | (None) | (2-5A) | (RIG-I Ligand) |
| UU$^{120}$ | 564 | 461 | 496 | 24 | 930 | 312 |
| UU$^{121}$ | 239 | 198 | 225 | 32 | 431 | 121 |
| UA$^{115}$ | 35 | 54 | 53 | 3 | 74 | 37 |
| UA$^{74}$ | 0 | 50 | 62 | 0 | 1 | 0 |
| GG$^{117}$ | 90 | 49 | 73 | 19 | 114 | 32 |
| GC$^{118}$ | 77 | 49 | 93 | 2 | 122 | 24 |
| CU$^{119}$ | 54 | 49 | 79 | 6 | 141 | 67 |
| AG$^{116}$ | 74 | 23 | 56 | 4 | 88 | 24 |
| GG$^{87}$ | 9 | 20 | 63 | 1 | 2 | 1 |
| GU$^{114}$ | 28 | 19 | 31 | 2 | 24 | 9 |

*Extended Data Tables 8: UMI-corrected cDNA reads in 5s rRNA*

* 10 most frequent cleavage sites (benchmarked to wild type macrophages treated with 2-5A).

Number of UMI reads corresponding to a cyclic phosphate at each position in 5S rRNA.

Red: 2-5A activated cleavage sites / RIG-I ligand activated cleavage sites / RNase L-dependent ≥ 10-fold activation in wild type macrophages and little-to-no activation in RNASE L -/- macrophages.

| | Wildtype Macrophage (treatment) | | | RNase L -/- Macrophage (treatment) | | |
|---|---|---|---|---|---|---|
| Position | (None) | (2-5A) | (RIG-I Ligand) | (None) | (2-5A) | (RIG-I Ligand) |
| UU$^{120}$ | 39.6 | 33.5 | 22.6 | 16.2 | 44.4 | 45.5 |
| UU$^{121}$ | 16.8 | 14.4 | 10.2 | 21.6 | 20.6 | 17.7 |
| UA$^{115}$ | 2.5 | 3.9 | 2.4 | 2.0 | 3.5 | 5.4 |
| UA$^{74}$ | 0.0 | 3.6 | 2.8 | 0.0 | 0.0 | 0.0 |
| GG$^{117}$ | 6.3 | 3.6 | 3.3 | 12.8 | 5.4 | 4.7 |
| GC$^{118}$ | 5.4 | 3.6 | 4.2 | 1.4 | 5.8 | 3.5 |
| CU$^{119}$ | 3.8 | 3.6 | 3.6 | 4.1 | 6.7 | 9.8 |
| AG$^{116}$ | 5.2 | 1.7 | 2.5 | 2.7 | 4.2 | 3.5 |
| GG$^{87}$ | 0.6 | 1.5 | 2.9 | 0.7 | 0.1 | 0.1 |
| GU$^{114}$ | 2.0 | 1.4 | 1.4 | 1.4 | 1.1 | 1.3 |

*Extended Data Tables 9: Percentage of cleavage at individual sites in 5s rRNA*

* 10 most frequent cleavage sites (benchmarked to wild type macrophages treated with 2-5A).

Percentage of cleavage at individual sites in 5s rRNA (% of UMI-corrected reads in 5s rRNA).

Red: 2-5A activated cleavage sites / RIG-I ligand activated cleavage sites / RNase L-dependent ≥ 10-fold activation in wild type macrophages and little-to-no activation in RNASE L -/- macrophages

| | Wildtype Macrophage (treatment) | | | RNase L -/- Macrophage (treatment) | | |
|---|---|---|---|---|---|---|
| Position | (None) | (2-5A) | (RIG-I Ligand) | (None) | (2-5A) | (RIG-I Ligand) |
| $UU^{107}$ | 1220 | 988 | 2138 | 94 | 500 | 209 |
| $UU^{106}$ | 143 | 119 | 206 | 5 | 30 | 39 |
| $UU^{105}$ | 43 | 42 | 73 | 1 | 25 | 19 |
| $UA^{102}$ | 34 | 23 | 36 | 0 | 11 | 7 |
| $UU^{104}$ | 29 | 23 | 69 | 1 | 18 | 5 |
| $AU^{103}$ | 30 | 22 | 49 | 1 | 12 | 2 |
| $CC^{99}$ | 9 | 10 | 10 | 7 | 3 | 6 |
| $AU^{101}$ | 27 | 8 | 22 | 0 | 6 | 4 |
| $CA^{100}$ | 12 | 7 | 17 | 0 | 5 | 7 |
| $AA^{83}$ | 3 | 3 | 3 | 0 | 0 | 0 |

*Extended Data Tables 10: UMI-corrected cDNA reads in U6 snRNA*

* 10 most frequent cleavage sites (benchmarked to wild type macrophages treated with 2-5A).

Number of UMI reads corresponding to a cyclic phosphate at each position in U6 snRNA.

| | Wildtype Macrophage (treatment) | | | RNase L -/- Macrophage (treatment) | | |
|---|---|---|---|---|---|---|
| Position | (None) | (2-5A) | (RIG-I Ligand) | (None) | (2-5A) | (RIG-I Ligand) |
| $UU^{107}$ | 78.2 | 79.0 | 80.6 | 85.4 | 81.8 | 69.0 |
| $UU^{106}$ | 9.2 | 9.5 | 7.8 | 4.5 | 4.9 | 12.9 |
| $UU^{105}$ | 2.8 | 3.4 | 2.8 | 0.9 | 4.1 | 6.3 |
| $UA^{102}$ | 2.2 | 1.8 | 1.4 | 0.0 | 1.8 | 2.3 |
| $UU^{104}$ | 1.9 | 1.8 | 2.6 | 0.9 | 2.9 | 1.7 |
| $AU^{103}$ | 1.9 | 1.8 | 1.8 | 0.9 | 2.0 | 0.7 |
| $CC^{99}$ | 0.6 | 0.8 | 0.4 | 6.4 | 0.5 | 2.0 |
| $AU^{101}$ | 1.7 | 0.6 | 0.8 | 0.0 | 1.0 | 1.3 |
| $CA^{100}$ | 0.8 | 0.6 | 0.6 | 0.0 | 0.8 | 2.3 |
| $AA^{83}$ | 0.2 | 0.2 | 0.1 | 0.0 | 0.0 | 0.0 |

*Extended Data Tables 11: Percentage of cleavage at individual sites in U6 snRNA*

* 10 most frequent cleavage sites (benchmarked to wild type macrophages treated with 2-5A).

Percentage of cleavage at individual sites in U6 snRNA (% of UMI-corrected reads in U6 snRNA).

| | | Wildtype Macrophage (treatment) | | | RNase L -/- Macrophage (treatment) | | |
|---|---|---|---|---|---|---|---|
| mRNA | UCSC Gene | None | 2-5A | RIG-I Ligand | None | 2-5A | RIG-I Ligand |
| Cxcl9 | uc008ycv.2 | 0 | 0 | 0 | 0 | 0 | 0 |
| Serpina3g | uc007owz.2 | 0 | 0 | 0 | 0 | 0 | 1 |
| Gbp5 | uc012cyv.1 | 0 | 0 | 0 | 0 | 1 | 0 |
| Cd69 | uc009efi.1 | 0 | 0 | 0 | 0 | 1 | 0 |
| Ccl5 | uc007kpi.2 | 0 | 0 | 0 | 0 | 1 | 0 |

*Extended Data Tables 12: UMI-corrected cDNA reads in mRNAs of interest*

# Chapter 4: Materials and Methods

*Mice and cells.*

All mice used were on an inbred C57BL/6 background, and C57BL/6 mice were purchased from the Jackson Laboratories. *Mavs*$^{-/-}$ mice (provided by M. Gale, Jr., University of Washington, Seattle, WA) were generated on a C57BL/6 background as previously described[69]. *Rnasel-/-* mice were generated as described[48] and backcrossed onto a C57Bl/6 background. BMDMs were harvested from leg bones and cultured in complete RPMI media supplemented with MCSF for 8 days. WT controls for all experiments were age-matched C57BL/6 mice. Mice used were 4-20 weeks old and littermates were used when available. All mice were maintained in accordance with guidelines of the University of Washington Institutional Animal Care and Use Committee. HEK293T cells were obtained from the ATCC. SV40 Large T antigen-immortalized fibroblasts were generated by retroviral transduction of primary MEFs. All cell lines tested negative for mycoplasma contamination.

*Cell treatments and analysis.*

RIG-I ligand was transcribed and purified *in vitro* as previously described using the T7 Megashortscript kit (Ambion)[72]. PU/UC A template sequence is available in Table 2.2. BMDMs were plated at a density of 0.7 x $10^6$ in 12-well plates for transfection. For transfections, 5 μg poly(I:C), and 1 μg RIG-I ligand were complexed with Lipofectamine 2000 (Life Technologies) at a ratio of 1 μg nucleic acid to 1 μl lipid in a final volume of 1 ml. Final concentrations of 30 μg/ml DMXAA (Sigma-Aldrich), 10 ng/ml LPS (Sigma Aldrich), 500 nM Thapsigargin (Life Technologies), and 2.5 μg/ml Tunicamycin (Santa Cruz Biotechnology) were added directly to the culture media. Treatment times are indicated in figures. For quantitative RT-PCR of IFN-β mRNA, cells were harvested into RNA-Bee (Teltest). RNA was treated with DNase (Ambion) and primed with Oligo(dT), then reverse transcribed with Superscript III (Life Technologies). cDNA was used for PCR with EVA Green reagents (Bio-Rad Laboratories) on a Bio-Rad CFX96 Real-Time System. The abundance of each cytokine mRNA was normalized to HPRT expression and compared with untreated cells transduced with the same shRNA to calculate the relative induction. Primers are available in Table 2.2.

*Lentiviral shRNA knockdown and CRISPR*

SKIV2L, TTC37 and control shRNA constructs were designed and cloned into the pLKO.1 vector. XRN1 shRNA was designed and cloned into the retroviral MSCV-LMP vector. SKIV2L was targeted by the sequence (sense): 5′-CGCATCATGGAGTCTGTGAAT-3′. TTC37 is targeted by a combination of two plasmids: (sense): 5′-AGAAGATTATGTGCCTGCCTT-3′ and (sense): 5′-TTCAGAATTCCGCTTCAGCTT-3′. XRN1 was targeted by the sequence (sense): 5′-GAGTAGCTTCTAGAGATAA-3′. The control shRNA targeted eGFP: 5′-CAACAAGATGAAGAGCACCAA-3′. Knockdowns were validated by immunoblotting of whole-cell extracts with mouse monoclonal antibodies according to standard techniques. Antibodies were: SKIV2L (Proteintech Group, Inc. catalog number 11462-1-AP), TTC37 (Abcam, catalog number ab122421), XRN1 (Santa Cruz Biotechnology, Catalog #sc-98459), and actin (Sigma, clone AC-74).

For SKIV2L, XRN1 and TTC37 knockdowns in BMDMs, VSV-G-pseudotyped lentivirus was produced by transfecting 2.5 x $10^6$ HEK293T cells in 10-cm plates with 10 μg of shRNA knockdown construct, 9 μg psPAX-2, a lentiviral packaging plasmid with a puromycin resistance gene, and 1 μg pVSV-G envelope plasmid for 48 h. 4 x $10^6$ BMDMs were transduced with HEK293T viral supernatants on days 3 and 4 after harvest, selected with 5 μg/ml puromycin (Life Technologies) for 3 d, and then plated for transfection (described above)

For CRISPR-Cas9 targeting of *Ern1*, we developed a lentivirus vector similar to the one recently reported by Zhang and colleagues[109] in which a U6 promoter-driven guide RNA and a MND promoter-driven Cas9-T2A-blasticidin resistance cassette were constitutively expressed from a single, self-inactivating lentivirus upon integration into the host cell genome. Immortalized MEFs were transduced and selected as described above, and CRISPR targeting of the *Ern1* locus was evaluated by restriction fragment length polymorphism (RFLP) using a restriction site that overlapped the CRISPR targeting site (IRE-1 guide 1: BsajI, IRE-1 guide 2: MlucI). Products were run on a 3% MetaPhor agarose gel (Lonza, Supplementary Figure 1). The sequences of the guide RNA target sequences are: IRE-1α gRNA #1 (sense): 5′-GCTTGTTGTTTGTCTCGACCC-3′; IRE-1α gRNA #2 (sense): 5′-GGGGAGGCCTGAACCAATTC-3′.

*Splicing Assay*

RT-PCR Xbp1 splicing assays were performed as described previously[85]. cDNA was obtained as described above. Product was amplified using sense primer mXBP1.3S (sense): 5'-AAACAGAGTAGCAGCGCAGACTGC-3', and antisense primer mXBP1.2AS (antisense): 5'-GGATCTCTAAAACTAGAGGCTTGGTG-3'. PCR products were then digested with PstI and run on a 3% MetaPhor agarose gel (Lonza).

*Human Interferon Signature Scores*

Human peripheral blood samples were obtained with informed, written consent, processed, and analyzed for the expression of six human interferon-stimulated genes as described previously [86]. AGS sample collection was approved by the Leeds (East) Research Ethics Committee (reference number 10/H1307/132). THES patient sample collection was approved by the South Birmingham Research Ethics Committee, and by the French ministry of Health, authorization number: AC-2011-1312.

*2-5A Synthesis*

2-5A synthesis using recombinant porcine OAS was done as described[110].

*Microarray Analysis and Deep Sequencing*

Microarray analysis was performed using Illumina Mouse WG-6 v 2.0 beadchips. Large scale 2-5A synthesis and HPLC purification of 2-5A species was performed as previously described[58]. Deep sequencing of 3' phosphate RNAs was done as described[100].

*Polysome Anylysis*

Polysome analysis was performed using standard techniques.

## Concluding Remarks

Managing the production of type I interferons is paramount to avoiding autoimmune disorders. This work considers the sources of endogenous nucleic acids and the importance of degrading them to maintain cellular homeostasis. We discover a novel negative regulator of the cell-intrinsic antiviral pathway, and we redefine a separate mechanism by which the antiviral response can block global translation and stop viral replication. Finally, we have preliminary evidence to suggest that antiviral proteins dedicated to sensing RNA viruses are in fact able to generate molecules that can directly activate sensors of the DNA-activated antiviral response.

The mechanisms of RNA metabolism, the detection of RNA viruses, and the unfolded protein response have all been well studied independently. However, crosstalk between these disparate pathways has not been previously considered. While work is ongoing on the finer points of how our immune system detects and responds to viral infection, our research provides a new context for how erroneous activation of these carefully regulated systems can have dire consequences for the host. In the case of SKIV2L, we have described how a helicase involved in generic RNA metabolism has a unique role in limiting both endogenous and exogenous nucleic acids. The IRE-1 dependent production of immunostimulatory nucleic acids is of little to no consequence when our RNA housekeeping machinery is intact. However, disruption of SKIV2L allows these molecules to accumulate to levels sufficient to activate the antiviral response. We propose that the relevance of this model is in human variants of SKIV2L where reduced function in highly secretory cells would lead to an accumulation of immunostimulatory endogenous RNAs. We hypothesize that this chronic, low-grade inflammation might be sufficient over time in these cells to attract an unwarranted immune response and lead to the break in tolerance that researchers have so far been unable to understand. This would help explain the onset of certain type I interferon-associated autoimmune disorders, though more work is necessary to confirm this connection.

While the OAS/2-5A system and RNase L have been studied for over 30 years, their role in the antiviral response has primarily been considered in the context of a model proposed 7 years ago. We began our studies on this system focusing on RNase L as another source of endogenous

immunostimulatory RNAs to evaluate its contribution alongside IRE-1. Our hypothesis was that RNase L knockout mice would be absent of these immunostimulatory RNAs, and anticipated that would provide a control for our SKIV2L experiments. When we did preliminary studies, we were alarmed to find that transfection of a RIG-I ligand had a greatly enhanced interferon response in RNase L knockout mice, which was at odds with the published model. Once experiments were repeated and confirmed, we reconsidered the roles RNase L and 2-5A play in the antiviral response. Microarray analysis further confirmed our observations that RNase L was not a positive regulator, but instead a negative regulator of the innate antiviral response.

2-5A has been described with a single biological relevance for its ability to bind to and activate RNase L. We were surprised, then, when we observed transfected 2-5A activate RLRs in the absence of RNase L, inducing IFN production. The OAS proteins in humans generate a variety of 2-5A species, and we decided to evaluate if there were distinct roles for each. We found that a 3mer, 4mer, and 5mer all acted in the same manner as our mixed prep of 2-5A to induce a robust RNase L-dependent type I interferon response. What we didn't anticipate was the 2-5A dinucleotide generating the same interferon response in wild type cells in an RNase L-independent manner. Most exciting was that this 2-5A dinucleotide was dependent on STING for this interferon induction, which presents the possibility for an important mechanism of crosstalk between the RNA and DNA sensing pathways.

The biological role of different OAS proteins has not been considered beyond their shared ability to make 2-5A. These different OASs generate different species of 2-5A, and we now know that these different 2-5As have distinct biological roles. This will change the way we think about the viral detection pathway. While the PRRs RIG-I and MDA5 have been studied as the sensors of the RNA antiviral response, there might be equally important and previously unconsidered roles for the OAS proteins in programming other pathways of the antiviral response.

These observations enhance our understanding of host defense pathways, while presenting new known sites of opportunity for viral proteins to antagonize the interferon response. There is also hope that these studies will increase our understanding of disease associated with polymorphisms in these genes. As discussed in our SKIV2L study, regulation of antiviral signaling pathways is essential to keep

potent and potentially damaging immune responses at bay. With a more complete awareness of OAS proteins as PRRs and 2-5A as a second messenger, we will better understand how the immune response to viral infection is shapes and where misregulation can lead to disease pathology. The conceptual advances suggested by our studies are exciting, but we are most excited for the new discoveries they inspire.

## References


1. Isaacs, A. & Lindenmann, J. Virus interference. I. The interferon. *Proc R Soc Lond B Biol Sci* **147**, 258-267 (1957).
2. Yoneyama, M. & Fujita, T. Recognition of viral nucleic acids in innate immunity. *Reviews in medical virology* **20**, 4-22, doi:10.1002/rmv.633 (2010).
3. Suresh, R. & Mosser, D. M. Pattern recognition receptors in innate immunity, host defense, and immunopathology. *Advances in physiology education* **37**, 284-291, doi:10.1152/advan.00058.2013 (2013).
4. Barbalat, R., Ewald, S. E., Mouchess, M. L. & Barton, G. M. Nucleic acid recognition by the innate immune system. *Annu Rev Immunol* **29**, 185-214, doi:10.1146/annurev-immunol-031210-101340 (2011).
5. Stetson, D. B., Ko, J. S., Heidmann, T. & Medzhitov, R. Trex1 prevents cell-intrinsic initiation of autoimmunity. *Cell* **134**, 587-598 (2008).
6. Aicardi, J. & Goutieres, F. A progressive familial encephalopathy in infancy with calcifications of the basal ganglia and chronic cerebrospinal fluid lymphocytosis. *Ann Neurol* **15**, 49-54 (1984).
7. Akira, S., Uematsu, S. & Takeuchi, O. Pathogen recognition and innate immunity. *Cell* **124**, 783-801 (2006).
8. Medzhitov, R. Recognition of microorganisms and activation of the immune response. *Nature* **449**, 819-826, doi:10.1038/nature06246 (2007).
9. Kato, H. *et al*. Differential roles of MDA5 and RIG-I helicases in the recognition of RNA viruses. *Nature* **441**, 101-105 (2006).
10. Wilkins, C. & Gale, M., Jr. Recognition of viruses by cytoplasmic sensors. *Curr Opin Immunol* **22**, 41-47, doi:10.1016/j.coi.2009.12.003 (2010).
11. Kawai, T. *et al*. IPS-1, an adaptor triggering RIG-I- and Mda5-mediated type I interferon induction. *Nat Immunol* **6**, 981-988 (2005).
12. Xu, L. G. *et al*. VISA Is an Adapter Protein Required for Virus-Triggered IFN-beta Signaling. *Mol Cell* **19**, 727-740 (2005).
13. Seth, R. B., Sun, L., Ea, C. K. & Chen, Z. J. Identification and characterization of MAVS, a mitochondrial antiviral signaling protein that activates NF-kappaB and IRF 3. *Cell* **122**, 669-682 (2005).
14. Baechler, E. C. *et al*. Interferon-inducible gene expression signature in peripheral blood cells of patients with severe lupus. *Proc Natl Acad Sci U S A* **100**, 2610-2615 (2003).
15. Theofilopoulos, A. N., Baccala, R., Beutler, B. & Kono, D. H. Type I interferons (alpha/beta) in immunity and autoimmunity. *Annu Rev Immunol* **23**, 307-336 (2005).
16. Banchereau, J. & Pascual, V. Type I interferon in systemic lupus erythematosus and other autoimmune diseases. *Immunity* **25**, 383-392 (2006).
17. Stark, G. R., Kerr, I. M., Williams, B. R., Silverman, R. H. & Schreiber, R. D. How cells respond to interferons. *Annu Rev Biochem* **67**, 227-264 (1998).
18. Bonjardim, C. A., Ferreira, P. C. & Kroon, E. G. Interferons: signaling, antiviral and viral evasion. *Immunol Lett* **122**, 1-11, doi:10.1016/j.imlet.2008.11.002 (2009).
19. Barbeito, M. S., Mathews, C. T. & Taylor, L. A. Microbiological laboratory hazard of bearded men. *Applied microbiology* **15**, 899-906 (1967).
20. Bousquet-Antonelli, C., Presutti, C. & Tollervey, D. Identification of a regulated pathway for nuclear pre-mRNA turnover. *Cell* **102**, 765-775 (2000).
21. Mitchell, P. & Tollervey, D. mRNA stability in eukaryotes. *Curr Opin Genet Dev* **10**, 193-198 (2000).
22. Schneider, C. & Tollervey, D. Threading the barrel of the RNA exosome. *Trends Biochem Sci* **38**, 485-493, doi:10.1016/j.tibs.2013.06.013 (2013).
23. Mitchell, P. & Tollervey, D. Musing on the structural organization of the exosome complex. *Nat Struct Biol* **7**, 843-846, doi:10.1038/82817 (2000).

24. Welch, W. J. Mammalian stress response: cell physiology, structure/function of stress proteins, and implications for medicine and disease. *Physiological reviews* **72**, 1063-1081 (1992).
25. Bernales, S., Papa, F. R. & Walter, P. Intracellular signaling by the unfolded protein response. *Annu Rev Cell Dev Biol* **22**, 487-508, doi:10.1146/annurev.cellbio.21.122303.120200 (2006).
26. Reimold, A. M. *et al.* Plasma cell differentiation requires the transcription factor XBP-1. *Nature* **412**, 300-307 (2001).
27. Calfon, M. *et al.* IRE1 couples endoplasmic reticulum load to secretory capacity by processing the XBP-1 mRNA. *Nature* **415**, 92-96 (2002).
28. Travers, K. J. *et al.* Functional and genomic analyses reveal an essential coordination between the unfolded protein response and ER-associated degradation. *Cell* **101**, 249-258 (2000).
29. Li, H., Korennykh, A. V., Behrman, S. L. & Walter, P. Mammalian endoplasmic reticulum stress sensor IRE1 signals by dynamic clustering. *Proc Natl Acad Sci U S A* **107**, 16113-16118, doi:10.1073/pnas.1010580107 (2010).
30. Ron, D. & Walter, P. Signal integration in the endoplasmic reticulum unfolded protein response. *Nat Rev Mol Cell Biol* **8**, 519-529, doi:10.1038/nrm2199 (2007).
31. Dong, B., Niwa, M., Walter, P. & Silverman, R. H. Basis for regulated RNA cleavage by functional analysis of RNase L and Ire1p. *RNA* **7**, 361-373 (2001).
32. Hollien, J. & Weissman, J. S. Decay of endoplasmic reticulum-localized mRNAs during the unfolded protein response. *Science* **313**, 104-107, doi:10.1126/science.1129631 (2006).
33. Malathi, K., Dong, B., Gale, M., Jr. & Silverman, R. H. Small self-RNA generated by RNase L amplifies antiviral innate immunity. *Nature* **448**, 816-819, doi:10.1038/nature06042 (2007).
34. Fernando, M. M. *et al.* Identification of two independent risk factors for lupus within the MHC in United Kingdom families. *PLoS Genet* **3**, e192, doi:10.1371/journal.pgen.0030192 (2007).
35. Eckard, S. C. *et al.* The SKIV2L RNA exosome limits activation of the RIG-I-like receptors. *Nat Immunol*, doi:10.1038/ni.2948 (2014).
36. Hartley, J. L. *et al.* Mutations in TTC37 cause trichohepatoenteric syndrome (phenotypic diarrhea of infancy). *Gastroenterology* **138**, 2388-2398, 2398 e2381-2382, doi:10.1053/j.gastro.2010.02.010 (2010).
37. Fabre, A. *et al.* Novel mutations in TTC37 associated with tricho-hepato-enteric syndrome. *Hum Mutat* **32**, 277-281, doi:10.1002/humu.21420 (2011).
38. Fabre, A. *et al.* SKIV2L mutations cause syndromic diarrhea, or trichohepatoenteric syndrome. *Am J Hum Genet* **90**, 689-692, doi:10.1016/j.ajhg.2012.02.009 (2012).
39. Fabre, A., Martinez-Vinson, C., Goulet, O. & Badens, C. Syndromic diarrhea/Tricho-hepato-enteric syndrome. *Orphanet journal of rare diseases* **8**, 5, doi:10.1186/1750-1172-8-5 (2013).
40. Fabre, A. *et al.* Syndromic (phenotypic) diarrhoea of infancy/tricho-hepato-enteric syndrome. *Archives of disease in childhood* **99**, 35-38, doi:10.1136/archdischild-2013-304016 (2014).
41. Flodstrom-Tullberg, M. *et al.* RNase L and double-stranded RNA-dependent protein kinase exert complementary roles in islet cell defense during coxsackievirus infection. *J Immunol* **174**, 1171-1177 (2005).
42. Samuel, M. A. *et al.* PKR and RNase L contribute to protection against lethal West Nile Virus infection by controlling early viral spread in the periphery and replication in neurons. *J Virol* **80**, 7009-7019, doi:10.1128/JVI.00489-06 (2006).
43. Lee, K. P. *et al.* Structure of the dual enzyme Ire1 reveals the basis for catalysis and regulation in nonconventional RNA splicing. *Cell* **132**, 89-100, doi:10.1016/j.cell.2007.10.057 (2008).
44. Carpten, J. *et al.* Germline mutations in the ribonuclease L gene in families showing linkage with HPC1. *Nat Genet* **30**, 181-184, doi:10.1038/ng823 (2002).
45. Casey, G. *et al.* RNASEL Arg462Gln variant is implicated in up to 13% of prostate cancer cases. *Nat Genet* **32**, 581-583, doi:10.1038/ng1021 (2002).
46. Jin, W., Wu, D. D., Zhang, X., Irwin, D. M. & Zhang, Y. P. Positive selection on the gene RNASEL: correlation between patterns of evolution and function. *Mol Biol Evol* **29**, 3161-3168, doi:10.1093/molbev/mss123 (2012).
47. Dong, B. & Silverman, R. H. 2-5A-dependent RNase molecules dimerize during activation by 2-5A. *J Biol Chem* **270**, 4133-4137 (1995).

48. Zhou, A. *et al*. Interferon action and apoptosis are defective in mice devoid of 2',5'-oligoadenylate-dependent RNase L. *EMBO J* **16**, 6355-6363, doi:10.1093/emboj/16.21.6355 (1997).
49. Kerr, I. M., Brown, R. E. & Ball, L. A. Increased sensitivity of cell-free protein synthesis to double-stranded RNA after interferon treatment. *Nature* **250**, 57-59 (1974).
50. Roberts, W. K., Clemens, M. J. & Kerr, I. M. Interferon-induced inhibition of protein synthesis in L-cell extracts: an ATP-dependent step in the activation of an inhibitor by double-stranded RNA. *Proc Natl Acad Sci U S A* **73**, 3136-3140 (1976).
51. Hornung, V., Hartmann, R., Ablasser, A. & Hopfner, K. P. OAS proteins and cGAS: unifying concepts in sensing and responding to cytosolic nucleic acids. *Nat Rev Immunol* **14**, 521-528, doi:10.1038/nri3719 (2014).
52. Kranzusch, P. J., Lee, A. S., Berger, J. M. & Doudna, J. A. Structure of human cGAS reveals a conserved family of second-messenger enzymes in innate immunity. *Cell reports* **3**, 1362-1368, doi:10.1016/j.celrep.2013.05.008 (2013).
53. Han, Y., Whitney, G., Donovan, J. & Korennykh, A. Innate immune messenger 2-5A tethers human RNase L into active high-order complexes. *Cell reports* **2**, 902-913, doi:10.1016/j.celrep.2012.09.004 (2012).
54. Sun, L., Wu, J., Du, F., Chen, X. & Chen, Z. J. Cyclic GMP-AMP synthase is a cytosolic DNA sensor that activates the type I interferon pathway. *Science* **339**, 786-791, doi:10.1126/science.1232458 (2013).
55. Burdette, D. L. *et al*. STING is a direct innate immune sensor of cyclic di-GMP. *Nature* **478**, 515-518, doi:nature10429 [pii]
10.1038/nature10429 (2011).
56. Ablasser, A. *et al*. cGAS produces a 2'-5'-linked cyclic dinucleotide second messenger that activates STING. *Nature* **498**, 380-384, doi:10.1038/nature12306 (2013).
57. Hovnanian, A. *et al*. The human 2',5'-oligoadenylate synthetase locus is composed of three distinct genes clustered on chromosome 12q24.2 encoding the 100-, 69-, and 40-kDa forms. *Genomics* **52**, 267-277, doi:10.1006/geno.1998.5443 (1998).
58. Morin, B. *et al*. High yield synthesis, purification and characterisation of the RNase L activators 5'-triphosphate 2'-5'-oligoadenylates. *Antiviral Res* **87**, 345-352, doi:10.1016/j.antiviral.2010.06.003 (2010).
59. You, F. *et al*. ELF4 is critical for induction of type I interferon and the host antiviral response. *Nat Immunol* **14**, 1237-1246, doi:10.1038/ni.2756 (2013).
60. Aguirre, S. *et al*. DENV inhibits type I IFN production in infected cells by cleaving human STING. *PLoS Pathog* **8**, e1002934, doi:10.1371/journal.ppat.1002934 (2012).
61. Pichlmair, A. & Reis e Sousa, C. Innate recognition of viruses. *Immunity* **27**, 370-383 (2007).
62. Kato, H. *et al*. Length-dependent recognition of double-stranded ribonucleic acids by retinoic acid-inducible gene-I and melanoma differentiation-associated gene 5. *J Exp Med* **205**, 1601-1610, doi:10.1084/jem.20080091
jem.20080091 [pii] (2008).
63. Stetson, D. B. & Medzhitov, R. Recognition of cytosolic DNA activates an IRF3-dependent innate immune response. *Immunity* **24**, 93-103 (2006).
64. Xiao, T. S. & Fitzgerald, K. A. The cGAS-STING Pathway for DNA Sensing. *Mol Cell* **51**, 135-139, doi:10.1016/j.molcel.2013.07.004 (2013).
65. Jin, T. *et al*. Structures of the HIN domain:DNA complexes reveal ligand binding and activation mechanisms of the AIM2 inflammasome and IFI16 receptor. *Immunity* **36**, 561-571, doi:10.1016/j.immuni.2012.02.014 (2012).
66. Liao, J. C. *et al*. Interferon-inducible protein 16: insight into the interaction with tumor suppressor p53. *Structure* **19**, 418-429, doi:10.1016/j.str.2010.12.015 (2011).
67. Civril, F. *et al*. Structural mechanism of cytosolic DNA sensing by cGAS. *Nature* **498**, 332-337, doi:10.1038/nature12305 (2013).
68. Crow, Y. J. *et al*. Mutations in the gene encoding the 3'-5' DNA exonuclease TREX1 cause Aicardi-Goutieres syndrome at the AGS1 locus. *Nat Genet* **38**, 917-920 (2006).

69. Gall, A. *et al*. Autoimmunity Initiates in Nonhematopoietic Cells and Progresses via Lymphocytes in an Interferon-Dependent Autoimmune Disease. *Immunity* **36**, 120-131, doi:S1074-7613(12)00008-8 [pii]
10.1016/j.immuni.2011.11.018 (2012).
70. Garneau, N. L., Wilusz, J. & Wilusz, C. J. The highways and byways of mRNA decay. *Nat Rev Mol Cell Biol* **8**, 113-126, doi:10.1038/nrm2104 (2007).
71. Brown, J. T., Bai, X. & Johnson, A. W. The yeast antiviral proteins Ski2p, Ski3p, and Ski8p exist as a complex in vivo. *Rna* **6**, 449-457 (2000).
72. Saito, T., Owen, D. M., Jiang, F., Marcotrigiano, J. & Gale, M., Jr. Innate immunity induced by composition-dependent RIG-I recognition of hepatitis C virus RNA. *Nature* **454**, 523-527, doi:nature07106 [pii]
10.1038/nature07106 (2008).
73. Roberts, Z. J. *et al*. The chemotherapeutic agent DMXAA potently and specifically activates the TBK1-IRF-3 signaling axis. *J Exp Med* **204**, 1559-1569, doi:jem.20061845 [pii]
10.1084/jem.20061845 (2007).
74. Conlon, J. *et al*. Mouse, but not human STING, binds and signals in response to the vascular disrupting agent 5,6-dimethylxanthenone-4-acetic acid. *J Immunol* **190**, 5216-5225, doi:10.4049/jimmunol.1300097 (2013).
75. Yamamoto, M. *et al*. Role of Adaptor TRIF in the MyD88-Independent Toll-Like Receptor Signaling Pathway. *Science* (2003).
76. Cox, J. S., Shamu, C. E. & Walter, P. Transcriptional induction of genes encoding endoplasmic reticulum resident proteins requires a transmembrane protein kinase. *Cell* **73**, 1197-1206 (1993).
77. Mori, K., Ma, W., Gething, M. J. & Sambrook, J. A transmembrane protein with a cdc2+/CDC28-related kinase activity is required for signaling from the ER to the nucleus. *Cell* **74**, 743-756 (1993).
78. Credle, J. J., Finer-Moore, J. S., Papa, F. R., Stroud, R. M. & Walter, P. On the mechanism of sensing unfolded protein in the endoplasmic reticulum. *Proc Natl Acad Sci U S A* **102**, 18773-18784, doi:10.1073/pnas.0509487102 (2005).
79. Gardner, B. M. & Walter, P. Unfolded proteins are Ire1-activating ligands that directly induce the unfolded protein response. *Science* **333**, 1891-1894, doi:10.1126/science.1209126 (2011).
80. Cox, J. S. & Walter, P. A novel mechanism for regulating activity of a transcription factor that controls the unfolded protein response. *Cell* **87**, 391-404 (1996).
81. Sidrauski, C., Cox, J. S. & Walter, P. tRNA ligase is required for regulated mRNA splicing in the unfolded protein response. *Cell* **87**, 405-413 (1996).
82. Hollien, J. *et al*. Regulated Ire1-dependent decay of messenger RNAs in mammalian cells. *J Cell Biol* **186**, 323-331, doi:10.1083/jcb.200903014 (2009).
83. Takahasi, K. *et al*. Nonself RNA-sensing mechanism of RIG-I helicase and activation of antiviral immune responses. *Mol Cell* **29**, 428-440, doi:10.1016/j.molcel.2007.11.028 (2008).
84. Cho, J. A. *et al*. The unfolded protein response element IRE1alpha senses bacterial proteins invading the ER to activate RIG-I and innate immune signaling. *Cell Host Microbe* **13**, 558-569, doi:10.1016/j.chom.2013.03.011 (2013).
85. Han, D. *et al*. IRE1alpha kinase activation modes control alternate endoribonuclease outputs to determine divergent cell fates. *Cell* **138**, 562-575, doi:10.1016/j.cell.2009.07.017 (2009).
86. Rice, G. I. *et al*. Assessment of interferon-related biomarkers in Aicardi-Goutieres syndrome associated with mutations in TREX1, RNASEH2A, RNASEH2B, RNASEH2C, SAMHD1, and ADAR: a case-control study. *Lancet neurology* **12**, 1159-1169, doi:10.1016/S1474-4422(13)70258-8 (2013).
87. Kerr, I. M. & Brown, R. E. pppA2'p5'A2'p5'A: an inhibitor of protein synthesis synthesized with an enzyme fraction from interferon-treated cells. *Proc Natl Acad Sci U S A* **75**, 256-260 (1978).
88. Zhou, A., Hassel, B. A. & Silverman, R. H. Expression cloning of 2-5A-dependent RNAase: a uniquely regulated mediator of interferon action. *Cell* **72**, 753-765 (1993).
89. Malathi, K. *et al*. RNase L releases a small RNA from HCV RNA that refolds into a potent PAMP. *Rna* **16**, 2108-2119, doi:rna.2244210 [pii]

10.1261/rna.2244210 (2010).
90. Rebouillat, D. & Hovanessian, A. G. The human 2',5'-oligoadenylate synthetase family: interferon-induced proteins with unique enzymatic properties. *J Interferon Cytokine Res* **19**, 295-308, doi:10.1089/107999099313992 (1999).
91. Hovanessian, A. G., Brown, R. E. & Kerr, I. M. Synthesis of low molecular weight inhibitor of protein synthesis with enzyme from interferon-treated cells. *Nature* **268**, 537-540 (1977).
92. Zhao, L. *et al*. Antagonism of the interferon-induced OAS-RNase L pathway by murine coronavirus ns2 protein is required for virus replication and liver pathology. *Cell Host Microbe* **11**, 607-616, doi:10.1016/j.chom.2012.04.011 (2012).
93. Zhang, R. *et al*. Homologous 2',5'-phosphodiesterases from disparate RNA viruses antagonize antiviral innate immunity. *Proc Natl Acad Sci U S A* **110**, 13114-13119, doi:10.1073/pnas.1306917110 (2013).
94. Ishikawa, H. & Barber, G. N. STING is an endoplasmic reticulum adaptor that facilitates innate immune signalling. *Nature* **455**, 674-678, doi:nature07317 [pii] 10.1038/nature07317 (2008).
95. Chakrabarti, A., Jha, B. K. & Silverman, R. H. New insights into the role of RNase L in innate immunity. *J Interferon Cytokine Res* **31**, 49-57, doi:10.1089/jir.2010.0120 (2011).
96. Kristiansen, H., Gad, H. H., Eskildsen-Larsen, S., Despres, P. & Hartmann, R. The oligoadenylate synthetase family: an ancient protein family with multiple antiviral activities. *J Interferon Cytokine Res* **31**, 41-47, doi:10.1089/jir.2010.0107 (2011).
97. Sun, Q. *et al*. The specific and essential role of MAVS in antiviral innate immune responses. *Immunity* **24**, 633-642 (2006).
98. Rebouillat, D., Hovnanian, A., Marie, I. & Hovanessian, A. G. The 100-kDa 2',5'-oligoadenylate synthetase catalyzing preferentially the synthesis of dimeric pppA2'p5'A molecules is composed of three homologous domains. *J Biol Chem* **274**, 1557-1565 (1999).
99. Schutz, K., Hesselberth, J. R. & Fields, S. Capture and sequence analysis of RNAs with terminal 2',3'-cyclic phosphates. *Rna* **16**, 621-631, doi:10.1261/rna.1934910 (2010).
100. Cooper, D. A., Jha, B. K., Silverman, R. H., Hesselberth, J. R. & Barton, D. J. Ribonuclease L and metal-ion-independent endoribonuclease cleavage sites in host and viral RNAs. *Nucleic Acids Res* **42**, 5202-5216, doi:10.1093/nar/gku118 (2014).
101. Kivioja, T. *et al*. Counting absolute numbers of molecules using unique molecular identifiers. *Nat Methods* **9**, 72-74, doi:10.1038/nmeth.1778 (2012).
102. Han, Y. *et al*. Structure of human RNase L reveals the basis for regulated RNA decay in the IFN response. *Science* **343**, 1244-1248, doi:10.1126/science.1249845 (2014).
103. Anger, A. M. *et al*. Structures of the human and Drosophila 80S ribosome. *Nature* **497**, 80-85, doi:10.1038/nature12104 (2013).
104. Wreschner, D. H., James, T. C., Silverman, R. H. & Kerr, I. M. Ribosomal RNA cleavage, nuclease activation and 2-5A(ppp(A2'p)nA) in interferon-treated cells. *Nucleic Acids Res* **9**, 1571-1581 (1981).
105. Silverman, R. H., Skehel, J. J., James, T. C., Wreschner, D. H. & Kerr, I. M. rRNA cleavage as an index of ppp(A2'p)nA activity in interferon-treated encephalomyocarditis virus-infected cells. *J Virol* **46**, 1051-1055 (1983).
106. Brennan-Laun, S. E., Ezelle, H. J., Li, X. L. & Hassel, B. A. RNase-L control of cellular mRNAs: roles in biologic functions and mechanisms of substrate targeting. *J Interferon Cytokine Res* **34**, 275-288, doi:10.1089/jir.2013.0147 (2014).
107. Wu, J. *et al*. Cyclic GMP-AMP is an endogenous second messenger in innate immune signaling by cytosolic DNA. *Science* **339**, 826-830, doi:10.1126/science.1229963 (2013).
108. Sonenberg, N. & Hinnebusch, A. G. Regulation of translation initiation in eukaryotes: mechanisms and biological targets. *Cell* **136**, 731-745, doi:10.1016/j.cell.2009.01.042 (2009).
109. Shalem, O. *et al*. Genome-scale CRISPR-Cas9 knockout screening in human cells. *Science* **343**, 84-87, doi:10.1126/science.1247005 (2014).
110. Turpaev, K., Hartmann, R., Kisselev, L. & Justesen, J. Ap3A and Ap4A are primers for oligoadenylate synthesis catalyzed by interferon-inducible 2-5A synthetase. *FEBS Lett* **408**, 177-181 (1997).